Immunogenicity and tumorigenicity of pluripotent stem cells

Kooreman, N.G.

Chapter 5

Pluripotent stem cell therapy for vascular disease

Gu, M.[*]*, Mordwinkin, N.M.*[*]*, Kooreman, N.G., Lee, J., Wu, H., Hu, S., Churko, J.M., Diecke, S., Burridge, P.W., He, C., et al. (2015). Pravastatin reverses obesity-induced dysfunction of induced pluripotent stem cell-derived endothelial cells via a nitric oxide-dependent mechanism.* **European Heart Journal,** *36, 806-816.*

[*] *authors contributed equally*

ABSTRACT

Aims

High-fat diet-induced obesity (DIO) is a major contributor to type II diabetes and micro- and macro-vascular complications leading to peripheral vascular disease (PVD). Metabolic abnormalities of induced pluripotent stem cell-derived endothelial cells (iPSC-ECs) from obese individuals could potentially limit their therapeutic efficacy for PVD. The aim of this study was to compare the function of iPSC-ECs from normal and DIO mice using comprehensive *in vitro* and *in vivo* assays.

Methods and results

Six-week-old C57Bl/6 mice were fed with a normal or high-fat diet. At 24 weeks, iPSCs were generated from tail tip fibroblasts and differentiated into iPSC-ECs using a directed monolayer approach. *In vitro* functional analysis revealed that iPSC-ECs from DIO mice had significantly decreased capacity to form capillary-like networks, diminished migration, and lower proliferation. Microarray and ELISA confirmed elevated apoptotic, inflammatory, and oxidative stress pathways in DIO iPSC-ECs. Following hindlimb ischaemia, mice receiving intramuscular injections of DIO iPSC-ECs had significantly decreased reperfusion compared with mice injected with control healthy iPSC-ECs. Hindlimb sections revealed increased muscle atrophy and presence of inflammatory cells in mice receiving DIO iPSC-ECs. When pravastatin was co-administered to mice receiving DIO iPSC-ECs, a significant increase in reperfusion was observed; however, this beneficial effect was blunted by co-administration of the nitric oxide synthase inhibitor, N^{ω}-nitro-l-arginine methyl ester.

Conclusion

This is the first study to provide evidence that iPSC-ECs from DIO mice exhibit signs of endothelial dysfunction and have suboptimal efficacy following transplantation in a hindlimb ischaemia model. These findings may have important implications for future treatment of PVD using iPSC-ECs in the obese population.

INTRODUCTION

Obesity is a rapidly growing threat to global healthcare, with 1.5 billion adults overweight and 400 million of them considered obese. Increasing evidence indicates a high-caloric high-fat diet is a significant risk factor for causing deleterious effects on metabolism and heart function, and has been strongly linked to the progression of heart disease and type 2 diabetes (Szendroedi and Roden 2009, Birse et al. 2010, Flegal et al. 2010). Dysglycaemia associated with obesity, insulin resistance and subsequent diabetes mellitus can lead to decreased nitric oxide (NO) bioavailability, endothelial nitric oxide synthase (eNOS) uncoupling, and increased levels of reactive oxygen species (ROS) (Du et al. 2006). Left unchecked, this oxidative stress can result in an increased production of pro-inflammatory cytokines, leading to oxidative DNA damage and the activation nof cellular apoptotic signals and pathways (Esposito et al. 2002, Galassetti 2012). The hallmark of endothelial dysfunction involved in obesity and its vascular complications is thought to be the result of interplay between apoptosis, inflammation, and oxidative stress, including a reduced bioavailability of NO (Hink et al. 2001). Statins are 3-hydroxy-3-methyl-glutaryl-CoA reductase inhibitors used primarily to lower cholesterol levels. Statins have also been shown to have beneficial effects on endothelial progenitor cells, improve endothelial function, increase NO production, augment neovascularization, and decrease ROS and inflammatory cytokines (Liu et al. 2012). In recent years, embryonic stem cell-derived endothelial cells (ESC-ECs) have been evaluated in models of myocardial infarction and hindlimb ischaemia as a potential therapeutic option to promote angiogenesis and neovascularization (Cho et al. 2007, Li et al. 2007, Yu et al. 2009). At present, therapies derived from ESCs are associated with significant ethical and political concerns. The recent discovery of induced pluripotent stem cells (iPSCs) has provided an alternative for the treatment of ischaemic vascular disease (Takahashi et al. 2007). However, little is known about the function of induced pluripotent stem cell-derived endothelial cells (iPSC-ECs) derived from obese or overweight individuals, specifically whether they exhibit properties of endothelial dysfunction and impaired vascular function similar to native ECs from these individuals. This could potentially limit the use of iPSC-ECs from patients with diabetes as a therapeutic option for peripheral vascular disease (PVD) unless coadminister with low-dose pravastatin therapy.

METHODS

Experimental animals

Animal study protocols were approved by the Animal Research Committee at Stanford University. All mice were obtained from The Jackson Laboratories (Bar Harbor, ME, USA), and quarantined for one week prior to the initiation of treatment. They were kept on a

12-hour light/dark cycle, and food and water were available ad libitum. For derivation of murine iPSCs, donor tail tip fibroblasts were isolated from 24-week old male C57Bl/6 mice fed a normal diet (10% kcal from fat; control mice) or high-fat diet (60% kcal from fat; DIO mice) beginning at 6 weeks of age (n=5/group; Jackson Laboratories, Bar Harbor, ME, USA) (Wang and Liao 2012). Recipient animals undergoing hindlimb ischemia surgery consisted of 10-12 week old male NOD/SCID mice. To verify the presence of diabetes, intraperitoneal (IP) glucose tolerance tests (GTT) and insulin tolerance tests (ITT) were performed as described previously (Bruning et al. 1997, Andrikopoulos et al. 2008). Donor animals were then euthanized. In order to serve as internal controls for comparisons with iPSC-ECs, aortic endothelial cells (aortic-ECs) were also isolated from both control and DIO mice as previously described (Kobayashi et al. 2005).

Derivation and culture of murine iPSCs

Murine tail tip fibroblasts were dissociated and isolated with collagenase type IV (Life Technologies, Grand Island, NY, USA) and maintained with Dulbecco's modified Eagle medium (DMEM) containing 10% fetal bovine serum (FBS), L- glutamine, 4.5 g/L glucose, 100 U/mL penicillin, and 100 g/mL streptomycin at 37°C, 20% O2, and 5% CO2 in a humidified incubator. Murine fibroblasts (passage 1-2) were reprogrammed using a codon optimized 4-in-1 lentiviral vector encoding Oct4, Klf4, Sox2, and c-Myc as previously described (Warlich et al. 2011). Murine iPSC clones were transferred to irradiated murine embryonic fibroblast (MEF) feeder layers and subsequently maintained in DMEM containing 20% FBS, L-glutamine, non-essential amino acids (NEAA), β-mercaptoethanol, and 10 ng/mL leukemia inhibitory factor (LIF) at 37°C, 5% O2, and 10% CO2 in a humidified incubator and passaged every 3-4 days with trypsin. After 2 passages, iPSCs were transferred onto Matrigel-coated plates for further expansion.

Characterization of murine iPSCs

The pluripotency potential of iPSCs was determined by immunohistochemical staining for markers of the three germ layers following embryoid body (EB) formation (Burridge et al. 2007). At day 30, differentiated EBs were fixed with 4% paraformaldehyde for 15 minutes, permeabilized with 0.2% Triton X-100 in phosphate-buffered saline (PBS) for 30 minutes, and blocked with 1% bovine serum albumin (BSA) in PBS for 1 hour. The cells were then incubated with primary antibodies specific for markers representing the three germ layers: β-III-tubulin (TUJ-1) for ectoderm, SOX17 for endoderm, and smooth muscle actin (SMA) for mesoderm (Abcam, Cambridge, MA, USA). In addition, RT-PCR was performed on RNA isolated from fibroblasts, iPSCs, and EBs to evaluate the expression of genes specific to the three germ layers. TaqMan primers (Life Technologies) for ectoderm (Gbx, TJF), endoderm (α- fetoprotein [AFP], Foxa2), and mesoderm (GATA4, GATA6, MLC, Nkx) were used in this study, with 18s used as the endogenous control (Supplemental Table 1). Karyotype

analyses of passage 15 tail tip fibroblast-derived iPSCs were performed at the Cytogenetics Laboratory in the Department of Pathology at Stanford Hospital and Clinics. Cells were treated with 0.1 mg/mL colcemid for induction of mitotic arrest and were subsequently harvested by trypsin dispersal, hypotonic shock, and fixation with 3:1 methanol:acetic acid. For each cell line, 20 metaphases were analyzed by the standard G-banding method.

In vitro monolayer endothelial differentiation of murine iPSCs

To induce endothelial differentiation, approximately $1x10^5$ undifferentiated iPSCs were seeded in each well of Matrigel-coated 6-well plates and cultured in differentiation medium containing RPMI and B-27 supplement minus insulin (Life Technologies) with 5 μM CHIR-99021 (a glycogen synthase kinase [GSK]-3 inhibitor; Selleck Chemicals, Houston, TX, USA) for 2 days, followed by RPMI and B-27 supplement minus insulin with 2 μM CHIR-99021 for 2 additional days. The medium was then changed to RPMI and B-27 supplement minus insulin with 50 ng/mL vascular endothelial growth factor (VEGF; R&D Systems, Minneapolis, MN, USA), 10 ng/mL fibroblast growth factor basic (FGFb; R&D Systems), and 10 μM Y-27632 (a rho-associated protein kinase [ROCK] inhibitor; Sigma-Aldrich, Saint Louis, MO, USA) for 3 days. For the subsequent 7 days, the medium was changed to RPMI and B-27 supplement (with insulin) with 50 ng/mL VEGF, 10 ng/mL FGFb, 10 μM Y-27632, and 1 μM SB 431542 (a transforming growth factor [TGF]-β inhibitor; Sigma-Aldrich). At day 14, iPSC-ECs were sorted for $CD31^+/CD144^+$ markers using FACS and expanded on 0.2% gelatin coated plates. After sorting, iPSC-ECs were cultured in EBM-2 Basal Medium supplemented with the EGM-2 BulletKit (Lonza, Basel, Switzerland) at 37°C, 20% O2, and 5% CO2 in a humidified incubator with medium changes every 48 hours, and cells were passaged once they reached 80-90% confluence. Murine iPSC- ECs used for in vitro and in vivo characterizations were between passages 3 and 5.

Immunofluorescence staining of cultured murine iPSCs and iPSC-ECs

Cells were fixed with 4% paraformaldehyde for 15 minutes, permeabilized with 0.2% Triton X-100 in PBS for 30 minutes, and blocked with 1% BSA in PBS for 1 hour. Cells were then stained with appropriate primary antibodies and AlexaFluor-conjugated secondary antibodies (Life Technologies) and co-stained with DAPI (Vector Laboratories, Burlingame, CA, USA). The primary antibodies for SSEA-1 (EMD Millipore), Oct3/4 (Santa Cruz Biotechnology, Santa Cruz, CA, USA), Sox2 (BioLegend, San Diego, CA, USA), c-Myc (Abcam), CD31 (Life Technologies), and CD144 (BD Biosciences) were used in the staining. Murine iPSC-ECs were also incubated with 10 μg/mL DiI-Ac-LDL (Life Technologies) at 37°C for 6 hours. After washing twice with PBS, DiI- Ac-LDL uptake was detected with fluorescence microscopy as previously described (Voyta et al. 1984). Imaging was performed on a Zeiss LSM510 Meta inverted confocal microscope and processed with ZEN microscope software

(Carl Zeiss, Oberkochen, Germany) at the Stanford University Neuroscience Microscopy Service facility.

Biological characterization of murine iPSC-ECs

To determine the characteristics of aortic-ECs and iPSC-ECs in vitro, the formation of cord-like structures was assessed by seeding cells in 24-well plates coated with Matrigel and incubating them at 37°C for 24 hours as previously described (Yamashita et al. 2000). Cell proliferation was measured using the BrdU Cell Proliferation Assay Kit according to the manufacturer's protocol (Cell Signaling Technology, Danvers, MA, USA). EC adhesion and migration/wound-healing were determined using assays as previously described (Liang et al. 2007, Reinhart-King 2008). Wound-healing assay images were quantified using ImageJ (National Institutes of Health, Bethesda, MD, USA). In vitro apoptosis analysis was performed in a hypoxia chamber to mimic ischemic conditions, and measured via terminal deoxynucleotidyl transferase dUTP nick end labeling (TUNEL) using the Fluorescein In Situ Cell Death Detection Kit (Roche Applied Science, Penzberg, Germany) according to the manufacturer's protocol. Measurement of cell culture supernatant nitrite levels was determined using a Griess Reagent System according to the manufacturer's protocol (Promega, Madison, WI, USA). Enzyme-linked immunosorbent assay (ELISA) was performed on control and DIO iPSC-ECs cultured under hypoxic conditions for 24 hours using a Mouse Inflammatory Cytokines Multi-Analyte ELISArray Kit (Qiagen, Valencia, CA, USA) following the manufacturer's instructions. For pravastatin treatment, the dose was determined by adding pravastatin daily into the cell culture medium at 0.1, 1, and 10μM concentrations. No effect was seen using the 0.1 μM concentration, while cell death occurred at the 10μM concentration. The most significant effects were observed using 1μM pravastatin. Therefore, for all in vitro experiments in this study, pravastatin was used at this dose.

Surgical model for hindlimb ischaemia and cell delivery

The surgical procedure for the induction of unilateral hindlimb ischaemia was performed following a previously published protocol (Limbourg et al. 2009). Briefly, mice were anesthetized in an induction chamber containing 1–2% isoflurane (Baxter HealthCare, Deerfield, IL, USA) in 100% oxygen at a flow rate of 1 L/min. Ischaemia was induced by two separate ligations of the femoral artery, one distal and one proximal to the origin of the deep femoral branch. Subsequently, the skin was closed using 5-0 Vicryl sutures. Following the operation, animals were randomized into seven groups (n = 10 per group) and each was administered a single gastrocnemius intramuscular (IM) injection containing: (i) 50 μL of 1 : 1 Matrigel/EBM2 (vehicle), (ii) vehicle plus intraperitoneal (IP) pravastatin co-administration daily, (iii) 1×10^6 pooled iPSC-ECs from control donors in 50 μL of 1 : 1 Matrigel/EBM2, (iv) 1×10^6 pooled iPSC-ECs from DIO donors in 50 μL of 1 : 1 Matrigel/EBM2, (v) a single injection of 1×10^6 pooled iPSC-ECs fromDIOdonors plus co-administration of pravastatin

(20 mg/kg body weight; injected volume, 0.02 mL/g body weight, IP), (vi) a single injection of 1×10^6 pooled iPSC-ECs from DIO donors pre-incubated with 1 mM pravastatin for 7 days, and (vii) a single injection of 1×10^6 pooled iPSC-ECs from DIO donors plus co-administration of pravastatin and NO synthase inhibitor N^w-nitro-L-arginine methyl ester (L-NAME) daily. Prior to cell injection, iPSC-ECs were labelled with Cell- Tracker CM-DiI cell-labelling solution (Life Technologies) according to themanufacturer's instructions sothat the injected cells couldbe visualized post-mortem (Weir et al. 2008). To inhibit NO synthesis, L-NAME was administered in the drinking water at a concentration of 1 mg/mL during days 1 through 14 post cell delivery. Laser Doppler imaging (LDI) was performed on Days 0, 3, 7, 10, and 14 following cell injection.

Determination of the SDS-resistant eNOS dimers and monomers

SDS-resistant eNOS dimers and monomers were assayed using low-temperature NuPAGE® Novex® 3-8% Tris-Acetate Protein Gels as described previously (Leber et al. 1999, Zou et al. 2002), but with modifications. After treatment, samples were harvested and added to NuPAGE® LDS Sample Buffer (4X) directly without boiling. Samples were subjected to SDS-PAGE on 3-8% gels, and the whole western blot system were kept in ice bath at 4°C throughout the running and transfer procedures. After transfer, PVDF membranes were incubated with first antibodies against Phospho-Akt (Ser473) (1:1000, cell signaling #9271), Akt (1:1000, cell signaling #9272), eNOS (1:1000; cell signaling #9586), Phospho-eNOS (Ser1177) (1:1000, cell signaling #9571), Phospho-eNOS (Thr495) (1:1000, cell signaling #9574) in 5% fat-free milk overnight at 4°C. The blot was further incubated with a second horseradish peroxidase conjugated antibody against rabbit IgG (1:3000, life technology # G-21234) for 45 minutes at room temperature. The protein bands were visualized using the ECL Chemiluminescent Substrate Reagent Kit according to the manufacturer's instructions. The intensity (area times density) of the individual bands was quantitated by densitometry (GS-700 Imaging Densitometer; Bio-Rad Laboratories Inc.). Background was subtracted from the calculated area.

Microarray hybridization, data acquisition, and analysis

Microarray hybridization and data acquisition were performed at the Stanford Protein and Nucleic Acid Facility. Total RNA was isolated from biological duplicates of control and DIO iPSC-ECs using the RNeasy Mini Plus Kit (Qiagen). From the RNA samples, cDNA was reverse transcribed, and cRNA was then transcribed and hybridized to GeneChip Mouse Genome 430 2.0 microarrays (Affymetrix, Santa Clara, CA, USA) and processed according to the manufacturer's instructions. The array was scanned using an Affymetrix GeneChip Scanner 3000 7G, and data were normalized and annotated using Affymetrix Expression Console software. Gene expression intensity was generated from raw files and normalized by Robust Multi-array Average (RMA) using Partek Genomics Suite (Partek, Saint Louis,

MO, USA). One-way ANOVA P-value (<0.05) and fold- change (>1.5) was applied to select the significant differentially expressed genes. Canonical pathway analysis in Ingenuity Pathway Analysis software (Ingenuity Systems, Redwood City, CA, USA) was used to perform the gene pathway enrichment. TM4 Microarray Software Suite (Dana-Farber Cancer Institute, Boston, MA, USA) was used for hierarchical clustering and generating heat maps for significant differentially expressed genes and pathways.

Quantitative reverse-transcription polymerase chain reaction (qRT-PCR)

qRT-PCR of iPSC-ECs was performed using RT^2 Profiler Murine Apoptosis and Oxidative Stress Arrays and RT^2 SYBR Green/ROX qPCR Master Mix (Qiagen) on an ABI StepOnePlus Real-Time PCR System (Applied Biosystems) using biological triplicates. For data analysis, the ΔΔCt method was used and fold-change was calculated for each gene (DIO versus control group).

Histology and immunofluorescence staining

Two weeks following induction of hindlimb ischemia, mice were euthanized, hindlimbs snap frozen in O.C.T. compound (Sakura Finetek, Tokyo, Japan) and cryosectioned for histological and immunofluorescence assessment. Samples were sectioned longitudinally at a thickness of 5μm. Representative tissue sections were processed for routine hematoxylin and eosin (H&E) staining and reviewed by a pathologist blinded to the study groups. Incorporation of exogenous cells into the microvasculature of the ischemic tissue was assessed using immunofluorescence for CM-DiI (Life Technologies). For capillary density, sections were stained with a FITC-conjugated primary antibody specific for CD31 (BD Biosciences) and co-stained with DAPI (Vector Laboratories). At least 5 tissue sections were analyzed for each animal, with 5 high-powered images taken for each tissue section using a Leica DM IL LED inverted microscope equipped with a Leica DFC500 digital camera and processed with Leica LAS EZ software (Leica Microsystems, Buffalo Grove, IL, USA) and Image J software (NIH, Bethesda, MD, USA).

Statistical analysis

Statistics were calculated using GraphPad Prism (GraphPad Software, La Jolla, CA, USA). In vitro data were obtained from at least three independent experiments. Statistical significance between two groups was determined by paired or unpaired Student's t-test. For simple comparison between groups, one-way ANOVA was applied if the data were normally distributed, otherwise nonparametric Kruskal–Wallis test was used. For drug treatment experiments, two-way ANOVA followed by Bonferroni or Tukey's post hoc tests were applied. P-values were considered statistically significant if $P<0.05$ and all actual P-value are shown in the figures. All data are expressed as mean+SD.

RESULTS

Reprogramming of fibroblasts from control and diet-induced obesity mice into induced pluripotent stem cells

A previously published study has demonstrated that iPSCs can be generated from individuals with type 1 diabetes (Maehr et al. 2009). However, this study did not report the reprogramming efficiency of these cells. Hence, to test whether there is an inherent difference in the capacity of fibroblasts from control and DIO mice to be reprogrammed into iPSCs, tail tip fibroblasts were isolated from 24-week-old C57Bl/6 mice fed either a normal (10 kcal% from fat) or high-fat (60 kcal% from fat) diet beginning at 6 weeks of age. At 24 weeks of age, high-fat DIO mice had significantly increased body weight ($P = 0.001$), fasting glucose ($P = 0.016$), and showed a significant decrease in glucose and insulin tolerance compared to control mice ($P < 0.0001$; Supplementary material, Figure S1A–D). Next, we successfully reprogrammed tail tip fibroblasts into murine iPSCs using a codon optimized 4-in-1 lentiviral vector encoding Oct-4, Klf4, Sox2, and c-Myc. On Day 15 after reprogramming, we mechanically dissociated the individual iPSC colonies and transferred them onto irradiated MEF feeder layers for clonal expansion into multiple cell lines (3 lines/mouse, 5 mice/group) (Figure 1A). All murine iPSC colonies stained positive for alkaline phosphatase, as well as pluripotency markers SSEA-1, Oct4, Sox2, and c-Myc (Figure 1B–D). Interestingly, reprogramming efficiency was significantly lower in iPSCs derived from DIO mice compared with those derived from control mice ($P = 0.003$; Figure 1E). Immunohistochemistry and real-time polymerase chain reaction (RT-PCR) confirmed that the established iPSC lines were able to form cells derived from all three germ layers in vitro, expressed markers specific for endoderm, ectoderm, and mesoderm (Supplementary material, Figure S2A and B and Table S1), and also maintained a normal karyotype after extended passage (Supplementary material, Figure S3A and B).

Control and diet-induced obesity induced pluripotent stem cells can be successfully differentiated into induced pluripotent stem cell-derived endothelial cells

Next, we successfully differentiated iPSCs (at passage 15) from control and DIO mice into iPSC-ECs via a chemically defined monolayer differentiation protocol (Figure 2A). On Day 10 after induction of differentiation, iPSC-ECs were stained using antibodies against CD31 and CD144 and subsequently sorted by FACS. Double positive ($CD31^+/CD144^+$) cells were then plated on 0.2% gelatin coated plates for further expansion and characterization. Isolated iPSC-ECs showed Dil-Ac-LDL uptake and stained positive for endothelial markers CD31 and CD144 (Figure 2B). Flow cytometry showed no significant difference in EC differentiation capacity between iPSCs generated from DIO mice or healthy mice (18.80+1.51% vs. 20.47+1.75%, respectively; $P = 0.28$) (Supplementary material, Figure S4).

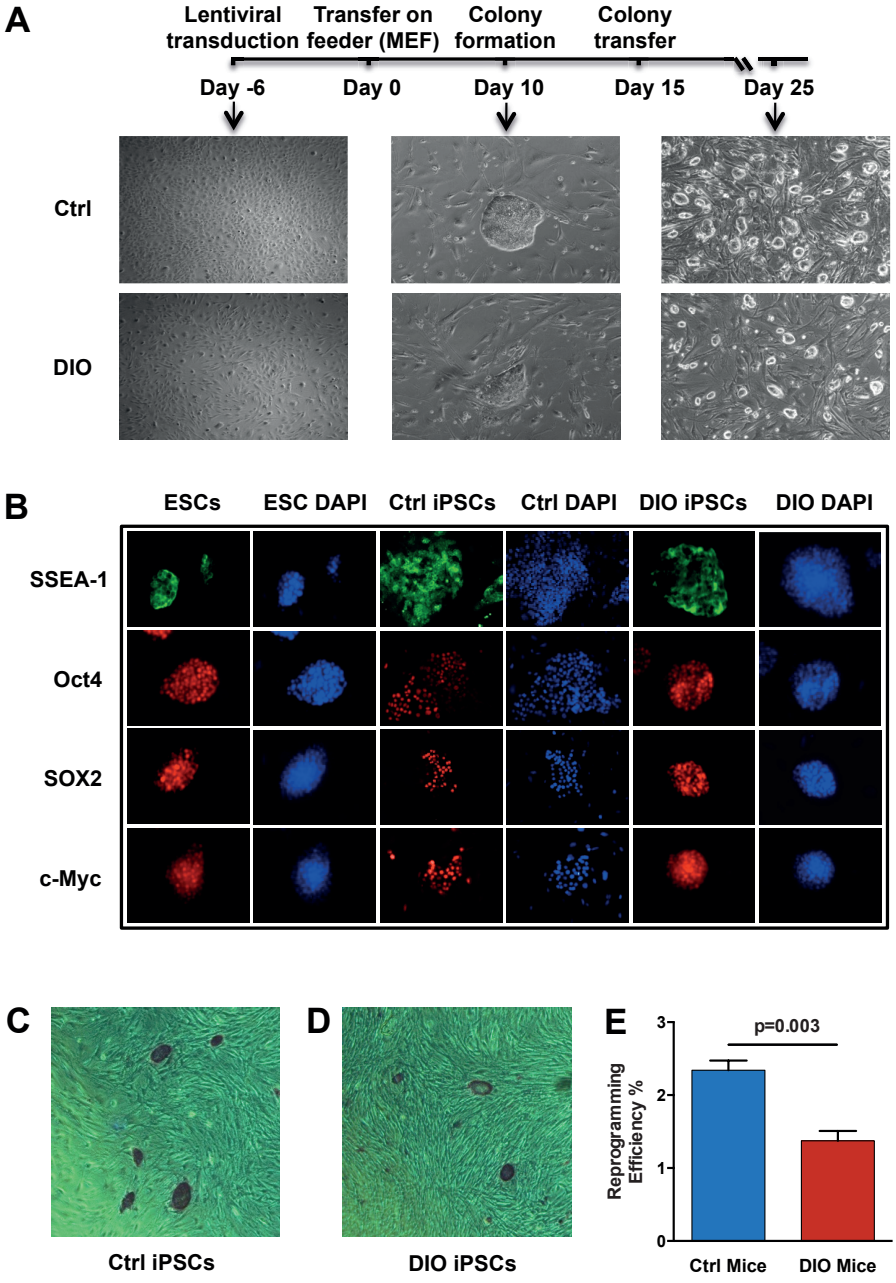

Figure 1. Generation and characterization of induced pluripotent stem cells. (A) Representative timeline of murine induced pluripotent stem cell generation. (B) Immunofluorescence of pluripotency markers SSEA-1, Oct4, Sox2, and c-Myc in mouse induced pluripotent stem cells. Mouse embryonic stem cells were used as positive control. (C–E) All murine induced pluripotent stem cell colonies stained positive for alkaline phosphatase. Reprogramming efficiency was significantly lower in induced pluripotent stem cells derived from diet-induced obesity tail tip fibroblasts compared with those derived from control mice (n = 5/group, P = 0.003).

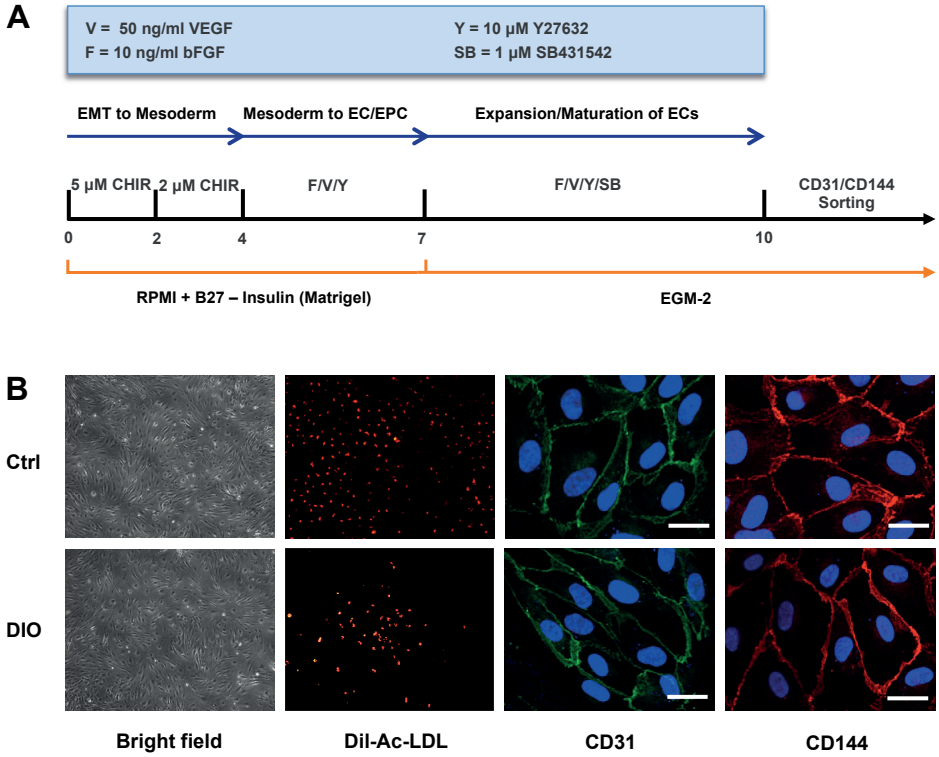

Figure 2. Differentiation of induced pluripotent stem cells into induced pluripotent stem cell-derived endothelial cells. (A) An outline of the protocol used for the differentiation of murine induced pluripotent stem cells to induced pluripotent stem cell-derived endothelial cells. At Day 14, induced pluripotent stem cell-derived endothelial cells were stained for CD31 and CD144, and double-positive ($CD31^+/CD144^+$) cells were expanded on 0.2% gelatin-coated plates in EGM-2 medium. (B) Representative brightfield images and positive immunofluorescence of differentiated induced pluripotent stem cell-derived endothelial cells for CD31 and CD144 at 63×. Differentiated induced pluripotent stem cell-derived endothelial cells also exhibited DiI-Ac-LDL uptake.

Diet-induced obesity induced pluripotent stem cell-derived endothelial cells exhibit endothelial dysfunction phenotype in vitro

Endothelial cells isolated from obese individuals have been shown to demonstrate properties of endothelial dysfunction in vitro (Caballero 2003). Similarly, we found cell migration and proliferation were significantly reduced among both aortic-ECs (data not shown) and iPSC-ECs from DIO mice compared with aortic-ECs and iPSC-ECs from control mice ($P < 0.05$; Figure 3A, B and E). Additionally, iPSC-ECs from DIO but not control mice showed a significant increase in apoptosis when cultured in a hypoxic environment ($P = 0.007$; Figure 3C and D). iPSC-ECs from DIO mice had significantly reduced capacity to form cord-like structures on Matrigel compared with control cells after 24 h ($P < 0.001$; Figure 3F). Incubation of iPSC-ECs from DIO mice with 1μM pravastatin for 24 h resulted in significant increases in cell migration ($P < 0.001$), proliferation ($P = 0.003$), and number of cord-like

structures on Matrigel ($P < 0.001$), and significant decrease in apoptosis ($P = 0.019$). Finally, DIO iPSC-ECs had significantly lower levels of NO production compared with control iPSC-ECs ($P = 0.019$); incubation of DIO iPSC-ECs with 1μM pravastatin for 24 h resulted in significantly higher levels of NO ($P = 0.016$). However, the effect of pravastatin in DIO iPSC-ECs was blocked by co-incubation with the NO synthase inhibitor L-NAME ($P = 0.001$) (Figure 3G). Interestingly, incubation of DIO iPSC-ECs with other statins including rosuvastatin (R-statin) and atorvastatin (A-statin) resulted in much less functional recovery compared with pravastatin (P-statin) (Supplementary material, Figure S5), which might be due to their different pharmacokinetic properties (Hamelin and Turgeon 1998).

Activation of Akt-endothelial nitric oxide synthase signalling pathway is suppressed in diet-induced obesity induced pluripotent stem cell-derived endothelial cells

As shown in Figure 3G, a hallmark of DIO iPSC-EC dysfunction was reduced NO production, which could be caused by reduced expression of endothelial or cytokine-inducible forms of NO synthase (eNOS and iNOS), impairment of eNOS activation, and/or increased eNOS uncoupling (Guzik 2002, Sansbury et al. 2012). Previous studies have shown that statins can rapidly promote the activation of Akt in endothelial cells leading to eNOS phosphorylation and increased NO production (Kureishi et al. 2000). To address our hypothesis that Akt and eNOS activation by statins was involved in improvement of DIO iPSC-EC function, we assessed eNOS and iNOS gene expressions as well as protein levels in control iPSC-ECs, DIO iPSC-ECs, and DIO iPSC-ECs with pravastatin preincubation. We found that DIO iPSC-ECs had significantly lower eNOS expression compared with control iPSC-ECs, which was reversed by pravastatin treatment for 24 h (Supplementary material, Figure S6A and B). Compared with eNOS expression, iNOS gene expression and protein levels were much lower in both control and DIO iPSC-ECs, suggesting a less important role in regulation of endothelial function (Supplementary material, Figure S7). We next assessed the modulation of Akt phosphorylation, eNOS phosphorylation, and eNOS coupling status by western blot analysis. A previous study showed that PKC signalling in endothelial cells inhibits eNOS activity by phosphorylating Thr-495 and dephosphorylating Ser-1177, whereas PKA signalling acts in reverse by increasing phosphorylation of Ser-1177 and dephosphorylation of Thr-495 to activate eNOS (Michell 2001). We found that iPSC-ECs from DIO mice showed significantly decreased phospho-Akt and phosphorylation of eNOS at the Ser1177 residue, which was reversed by pravastatin treatment. In contrast, the phosphorylation of eNOS at the Thr495 residue in DIO iPSC-ECs was significantly increased compared with control iPSC-ECs, indicating the deactivation of eNOS is associated with DIO (Supplementary material, Figure S6A, C–E). Finally, the percentage of the dimer-to-monomer ratio, an indicator of eNOS uncoupling which could lead to reduction of enzymatic activity (Rodríguez-Crespo et al. 1997, Zou et al. 2002), also showed a significant

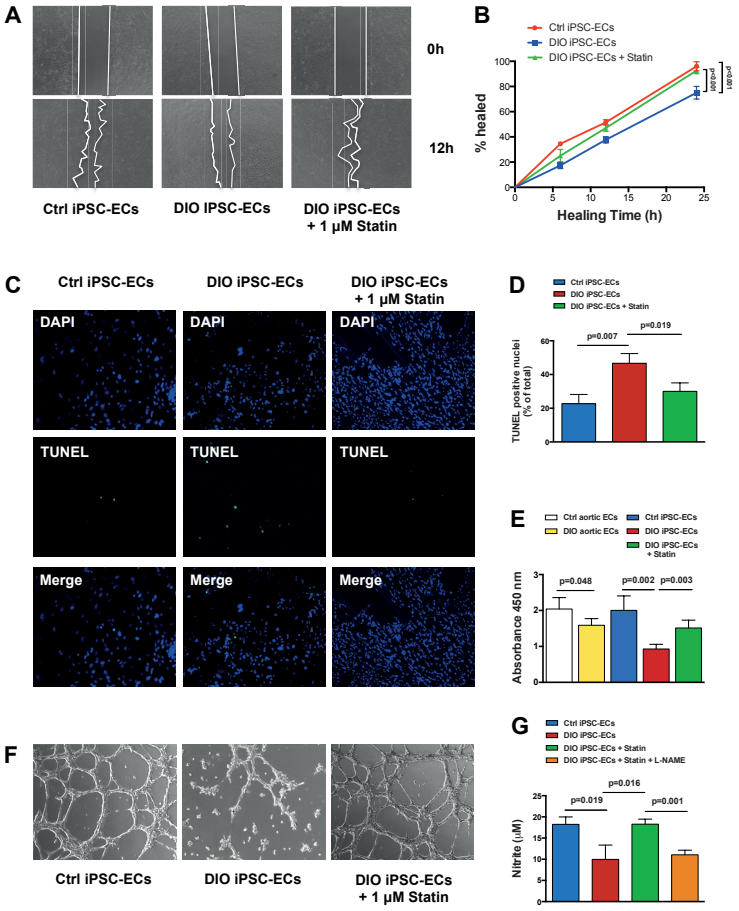

Figure 3. Characterization of induced pluripotent stem cell-derived endothelial cells in vitro. (A and B) Induced pluripotent stem cell-derived endothelial cells from diet-induced obesity mice demonstrated significant reduction in cell migration ($P < 0.001$). (C and D) TUNEL staining of diet-induced obesity induced pluripotent stem cell-derived endothelial cells demonstrated significant increase in apoptosis compared with control induced pluripotent stem cell-derived endothelial cells when cultured in hypoxic conditions ($P = 0.007$). (E) Both aortic-endothelial cells and induced pluripotent stem cell-derived endothelial cells from diet-induced obesity mice showed significant decrease in cell proliferation compared with control mice ($P = 0.048$ in aortic endothelial cells; $P = 0.002$ in induced pluripotent stem cell-derived endothelial cells). (F) Diet-induced obesity induced pluripotent stem cell-derived endothelial cells also demonstrated a reduced capacity to form cord-like network on Matrigel after 24 h compared with control induced pluripotent stem cell-derived endothelial cells ($P < 0.001$). The addition of 1 μM pravastatin to diet-induced obesity induced pluripotent stem cell-derived endothelial cells for 24 h resulted in significant increases in cell migration ($P < 0.001$), proliferation ($P = 0.003$), and the number of cord-like structures ($P < 0.001$), while significantly decreasing endothelial cell apoptosis ($P = 0.019$). (G) Measurement of nitrite levels in cell culture supernatant by Griess reaction demonstrated that diet-induced obesity induced pluripotent stem cell-derived endothelial cells had significantly lower levels of nitric oxide production compared with control induced pluripotent stem cell-derived endothelial cells ($P = 0.019$). Incubation of diet-induced obesity induced pluripotent stem cell-derived endothelial cells with 1 μM pravastatin for 24 h resulted in significantly higher levels of nitric oxide ($P = 0.016$). The effect of pravastatin on nitrite levels in diet-induced obesity induced pluripotent stem cell-derived endothelial cell was blocked by co-incubation with N^{ω}-nitro-l-arginine methyl ester ($P = 0.001$).

decrease in DIO iPSC-ECs, and was increased by pravastatin treatment (Supplementary material, Figure S6A, F).

Elevated apoptotic, inflammatory, and oxidative stress pathways in diet-induced obesity induced pluripotent stem cell-derived endothelial cells

Previous studies have shown endothelial dysfunction in patients with obesity is in part related to increased levels of oxidative stress, inflammation, cell apoptosis, and decreased NO production (Bruyndonckx et al. 2013). In order to investigate the mechanisms underlying the in vitro functional differences observed between DIO iPSC-ECs and control iPSC-ECs, we next performed microarray analysis. Our results indicate that 472 genes were differentially regulated in pathways related to apoptosis, inflammation, oxidative stress, and cellular senescence (Figure 4A; Supplementary material, Figure S8). We performed RT-PCR on a panel of genes involved in apoptosis and oxidative stress in control iPSC-ECs, DIO iPSC-ECs, and DIO iPSC-ECs after 1μM pravastatin treatment for 24 h. Of the genes investigated in these panels, 33 were significantly up-regulated (>three-fold) in DIO iPSC-ECs when compared with control iPSC-ECs (Figure 4B; Supplementary material, Table S2A and B). After pravastatin treatment, 28 apoptotic and oxidative genes were down-regulated in DIO iPSC-ECs. We next performed ELISA assays to determine levels of pro- and anti-inflammatory cytokines in cell culture supernatants following hypoxia for 24 h to mimic an ischaemic environment. Compared with control iPSC-ECs, DIO iPSC-ECs had significantly higher levels of inflammatory cytokines, including IL-1α, IL-1β, IL-4, IFN-γ, and TNF-α. Similarly, incubation of DIO iPSC-ECs with 1μM pravastatin for 24 h resulted in significant decreases in the pro-inflammatory cytokines IL-1α, IL-1β, IL-4, and TNF-α, as well as significant increases in the anti-inflammatory cytokines IL-6, IL-10, and IL 17A (Supplementary material, Figure S9).

Dysfunction of diet-induced obesity induced pluripotent stem cell-derived endothelial cells in a hindlimb ischaemia model is reversed by pravastatin co-administration

Several groups have demonstrated that healthy iPSC-ECs are effective in promoting angiogenesis and neovascularization in a hindlimb ischaemia model (Huang et al. 2010, Lai et al. 2013). However, it is unknown if DIO iPSC-ECs will also function properly in vivo. To characterize the functional differences between iPSC-ECs from control and DIO mice, we next induced hindlimb ischaemia and used LDI to quantify perfusion. Mice were randomized into seven groups (n = 10 per group) and each was administered a single gastrocnemius IM injection of a different treatment regimen (see Supplementary material). Beginning at Day 7 post-surgery, mice injected with control iPSC-ECs showed a significant increase in hindlimb reperfusion compared with mice injected with vehicle (0.38±0.04 vs. 0.61±0.04, vehicle vs. Ctrl iPSC-ECs, $P < 0.001$) or pravastatin only (0.45±0.06 vs. 0.61±0.04, vehicle

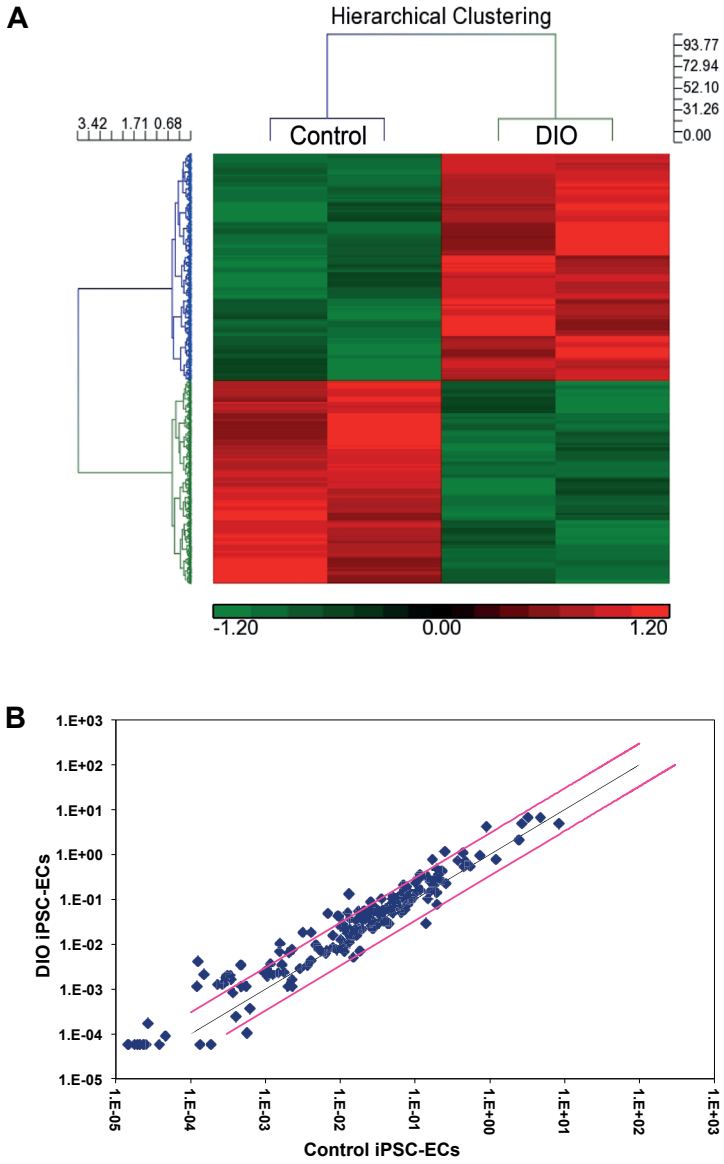

Figure 4. Microarray and RT-PCR gene expression profiling of induced pluripotent stem cell-derived endothelial cells from control and diet-induced obesity mice. (A) Heat map of the 472 significantly differentially regulated genes between diet-induced obesity induced pluripotent stem cell-derived endothelial cells and control induced pluripotent stem cell-derived endothelial cells. Enriched pathway analysis identified the involvement of biological pathways including metabolism, cell cycle, immune function, inflammation, cell adhesion, oxidative stress, senescence, and apoptosis. (B) RT-PCR for a panel of genes involved in apoptosis and cellular oxidative demonstrated a significant increase in many of these genes in diet-induced obesity induced pluripotent stem cell-derived endothelial cells compared with control induced pluripotent stem cell-derived endothelial cells (n = 5/group). Data expressed as fold-change with the black line indicating a one-fold-change and pink line indicating a three-fold change.

+ statin vs. Ctrl iPSC-ECs, P = 0.001) (Figure 5A and B). However, animals injected with DIO iPSC-ECs achieved significantly less hindlimb reperfusion compared with animals injected with control iPSC-ECs (0.61±0.04 vs. 0.46±0.06, Ctrl iPSC-ECs vs. DIO iPSC-ECs, P = 0.002). In addition, mice randomized to receive DIO iPSC-ECs combined with daily IP administration of pravastatin (beginning at Day 7) and mice randomized to receive DIO iPSC-ECs pre-incubated with pravastatin (beginning at Day 10) both had significantly higher levels of hindlimb reperfusion compared with mice that received DIO iPSC-ECs alone (Day 7: 0.62±0.02 vs. 0.46±0.06, DIO iPSC-ECs + IP statin vs. DIO iPSC-ECs, P < 0.001; Day 10: 0.66±0.04 vs. 0.53±0.02, DIO iPSC-ECs + prestatin vs.DIO iPSC-ECs, P = 0.004), and the level of perfusion was similar to that of mice receiving control iPSC-ECs. When mice that received DIO iPSC-ECs plus daily pravastatin also received the NO synthase inhibitor L-NAME in their drinking water, the increases in hindlimb reperfusion were significantly blunted from Day 7 onwards (0.62±0.02 vs. 0.54±0.09, DIO iPSC-ECs + IP statin vs. DIO iPSC-ECs + statin + L-NAME, P = 0.004), suggesting that the effect of pravastatin was via an NO-dependent pathway. Finally, we found that starting at Day 7, mice that received DIO iPSC-ECs combined with pravastatin treatment (either systemic treatment or pre-incubation) showed better hindlimb reperfusion than mice receiving pravastatin alone (0.45±0.06 vs. 0.62±0.02, vehicle + statin vs. DIO iPSC-ECs + IP statin, P < 0.001; 0.45±0.06 vs. 0.57±0.03, vehicle + statin vs. DIO iPSC-ECs + pre statin, P = 0.019), confirming the necessity of co-administration of pravastatin with DIO iPSC-ECs.

Histological evaluation of ischaemic hindlimbs confirms an apoptotic and inflammatory phenotype

We next performed histological evaluation of the ischaemic hindlimbs on Day 14 following cell injections. Hematoxylin & eosin (H&E) stained sections of hindlimbs from mice injected with DIO iPSC-ECs showed evidence of muscle atrophy and degeneration, as well as infiltration of inflammatory cells. In contrast, animals injected with control iPSC-ECs or DIO iPSC-ECs plus daily IP injections of pravastatin were protected from this damage. Animals injected with pre-treated DIO iPSC-ECs also showed reduced infiltration of neutrophils; however, the difference between DIO iPSC-ECs and DIO iPSC-ECs pre-treated with pravastatin did not reach statistical significance (P = 0.112) (Figure 6A and C). Immunostaining revealed that $CD31^+$ capillary density was significantly lower in the hindlimbs of mice injected with DIO iPSC-ECs compared with control iPSC-ECs (P = 0.006) (Figure 6B and D). Increased $CD31^+$ capillary density was observed in mice injected with DIO iPSC-ECs plus daily IP injections of pravastatin compared with mice injected with DIO iPSC-ECs alone (P = 0.047). Co-administration of the NO synthase inhibitor L-NAME with pravastatin blocked this effect (P = 0.001). Moreover, there was a trend showing that injection of DIO iPSC-ECs pre-treated with pravastatin for 7 days could also increase the capillary density compared with injection of untreated DIO iPSC-ECs; however, this did not

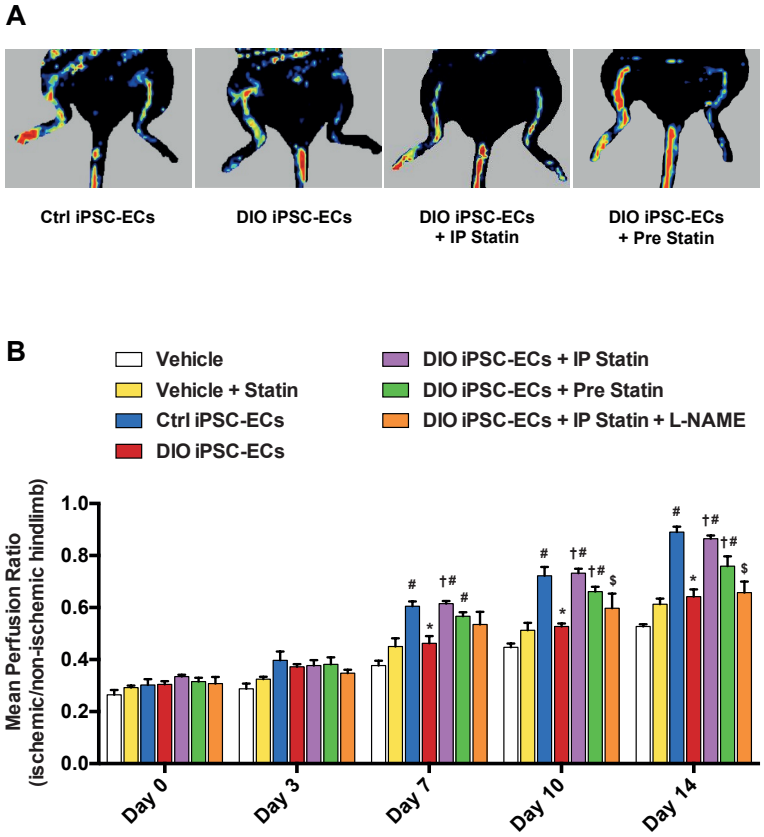

Figure 5. Laser Doppler imaging of ischaemic hindlimbs following intramuscular injection with vehicle, control induced pluripotent stem cell-derived endothelial cells, diet-induced obesity induced pluripotent stem cell-derived endothelial cells, and diet-induced obesity induced pluripotent stem cell-derived endothelial cells with treatments. (A) Graphic representation and (B) quantification by laser Doppler imaging show a significant increase in perfusion in the affected hindlimbs of mice injected with 1×10^6 control induced pluripotent stem cell-derived endothelial cells compared with vehicle alone and vehicle plus statin beginning at Day 7 post-injection ($P < 0.001$ vehicle vs. Ctrl induced pluripotent stem cell-derived endothelial cells; $P = 0.001$ vehicle + statin vs. Ctrl induced pluripotent stem cell-derived endothelial cells). Mice injected with 1×10^6 diet-induced obesity induced pluripotent stem cell-derived endothelial cells had a significant reduction in hindlimb perfusion compared with mice injected with control induced pluripotent stem cell-derived endothelial cells beginning at Day 7 post-injection ($P = 0.002$). Co-administration of pravastatin 20 mg/kg via daily intraperitoneal injections resulted in a significant increase in hindlimb reperfusion in mice that received diet-induced obesity induced pluripotent stem cell-derived endothelial cells starting from Day 7 ($P < 0.001$), while co-administration of N^{ω}-nitro-l-arginine methyl ester in these mice blocked this effect ($P = 0.004$). Injection with diet-induced obesity induced pluripotent stem cell-derived endothelial cells pre-treated with pravastatin in vitro also resulted in a significant increase in hindlimb reperfusion compared with injection of untreated diet-induced obesity induced pluripotent stem cell-derived endothelial cells starting from Day 10 ($P = 0.004$). n = 10/group, '†' vs. diet-induced obesity induced pluripotent stem cell-derived endothelial cells, "#" vs. vehicle + statin, "*" vs. control induced pluripotent stem cell-derived endothelial cells, "$" vs. diet-induced obesity induced pluripotent stem cell-derived endothelial cells + intraperitoneal statin

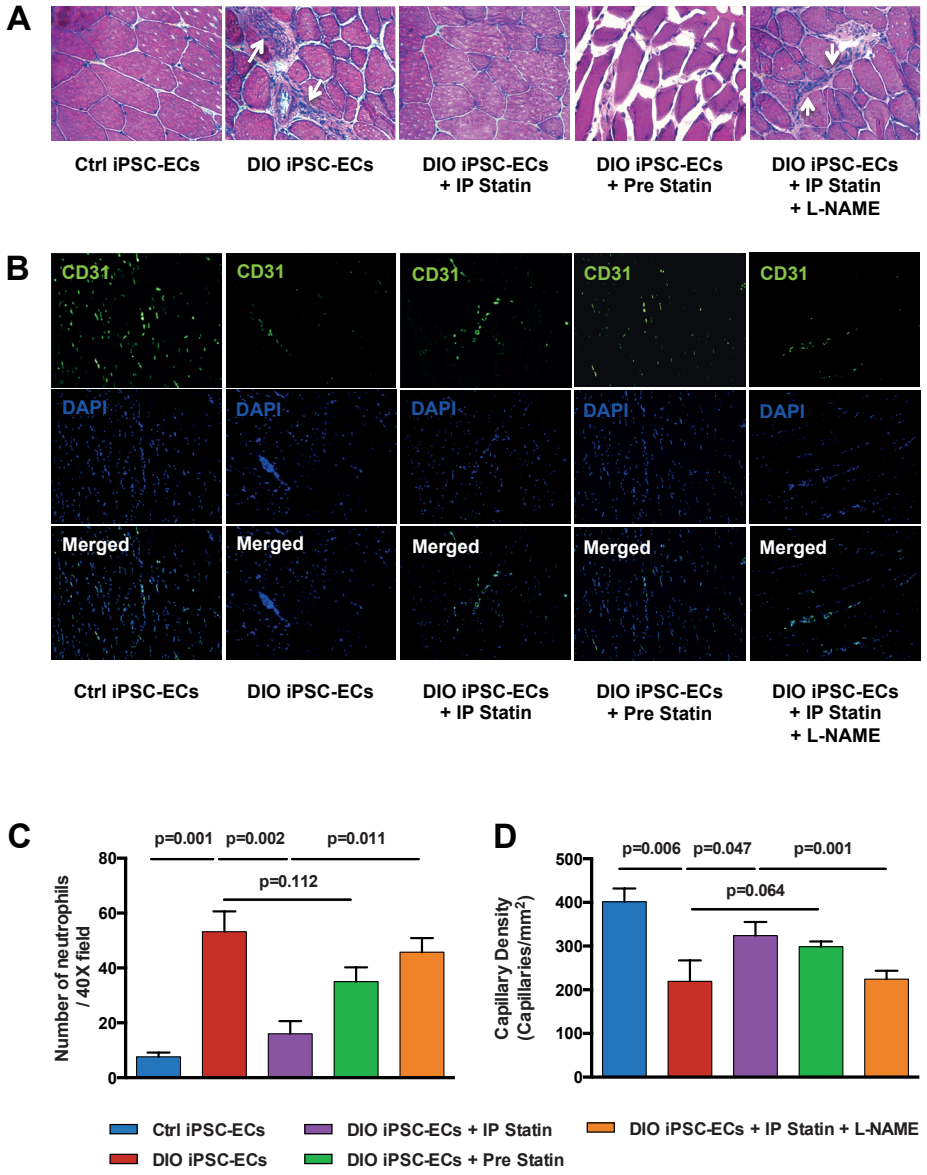

Figure 6. Histological evaluation of transplanted induced pluripotent stem cell-derived endothelial cells in the ischaemic hindlimb at Day 14.

Figure 6. Histological evaluation of transplanted induced pluripotent stem cell-derived endothelial cells in the ischaemic hindlimb at Day 14.
(A) H&E staining revealed evidence of muscle degeneration and inflammatory cell infiltration (indicated by white arrows) in animals injected with diet-induced obesity induced pluripotent stem cell-derived endothelial cells compared with animals injected with control induced pluripotent stem cell-derived endothelial cells, whereas animals injected with diet-induced obesity induced pluripotent stem cell-derived endothelial cells with intraperitoneal pravastatin treatment were protected from this damage. Co-administration of the nitric oxide inhibitor N^{ω}-nitro-l-arginine methyl ester blocked the effect of pravastatin in mice receiving diet-induced obesity induced pluripotent stem cell-derived endothelial cells (images at 40×). (B) Representative images of hindlimb frozen sections stained with mouse CD31 antibody. (C) Infiltration of the inflammatory cells was quantified by counting the number of neutrophils per high power field (40×). Three fields/animal and n = 5 animals per group were counted. Mice receiving diet-induced obesity induced pluripotent stem cell-derived endothelial cells showed significantly more neutrophil infiltration compared with mice injected with control induced pluripotent stem cell-derived endothelial cells (8 ± 2 vs. 54 ± 8, Ctrl induced pluripotent stem cell-derived endothelial cells vs. diet-induced obesity induced pluripotent stem cell-derived endothelial cells, P = 0.001), which was reversed by co-administration of diet-induced obesity induced pluripotent stem cell-derived endothelial cells and intraperitoneal pravastatin (54 ± 8 vs. 17 ± 5, diet-induced obesity induced pluripotent stem cell-derived endothelial cells vs. diet-induced obesity induced pluripotent stem cell-derived endothelial cells + intraperitoneal statin, P = 0.002). When mice that received diet-induced obesity induced pluripotent stem cell-derived endothelial cells plus daily pravastatin also received the nitric oxide synthase inhibitor N^{ω}-nitro-l-arginine methyl ester in their drinking water, the decrease in neutrophil infiltration was significantly blunted (17 ± 5 vs. 44 ± 5, diet-induced obesity induced pluripotent stem cell-derived endothelial cells + intraperitoneal statin vs. diet-induced obesity induced pluripotent stem cell-derived endothelial cells + intraperitoneal statin + N^{ω}-nitro-l-arginine methyl ester, P = 0.011). (D) Quantification of $CD31^{+}$ staining showed decreased number of capillaries per high power field in the hindlimbs of mice receiving diet-induced obesity induced pluripotent stem cell-derived endothelial cells compared with mice receiving control induced pluripotent stem cell-derived endothelial cells (P = 0.006). Co-administration of diet-induced obesity induced pluripotent stem cell-derived endothelial cells with pravastatin for 14 days resulted in a significant increase in capillary density compared with diet-induced obesity induced pluripotent stem cell-derived endothelial cells alone (P = 0.047), while co-administration of pravastatin with N^{ω}-nitro-l-arginine methyl ester blocked the effect of pravastatin in animals administered diet-induced obesity induced pluripotent stem cell-derived endothelial cells (P = 0.001).

reach statistical significance (P = 0.064). Immunofluorescent staining for CM-DiI-labelled iPSC-ECs verified engraftment of control iPSC-ECs in the ischaemic hindlimbs at Day 14 (Supplementary material, Figure S10). There was less detectable fluorescent signal in sectioned ischaemic hindlimbs of mice injected with labelled DIO iPSC-ECs compared with mice injected with DIO iPSC-ECs combined with daily IP injections of pravastatin.

DISCUSSION

Following hindlimb ischaemia injury, transplantation of ESC-ECs or iPSC-ECs can result in their incorporation into the host vasculature and increase reperfusion (Cho et al. 2007, Yamahara et al. 2008, Yu et al. 2009). However, since cells used in these studies were derived from healthy donors, it remains unknown if iPSC-ECs derived from DIO donors will function in the same way. Since patients who will require intervention to restore normal perfusion are likely to have significant morbidity such as obesity, identifying, and reversing endothelial dysfunction would be important before future application in regenerative medicine. The current study is the first to compare the functional capacity of iPSC-ECs from control healthy mice vs. DIO mice in vitro and in vivo. We first showed that DIO iPSC-ECs had impaired function in vitro compared with control iPSC-ECs. DIO iPSC-ECs had a reduced capacity to form cord-like structures on Matrigel after 24 h, as well as decreased migration and proliferation in vitro. When cultured in hypoxic conditions, DIO iPSC-ECs showed an increase in apoptosis compared with control iPSC-ECs. Second, by using a murine hindlimb ischaemia model, we showed that DIO iPSC-ECs exhibit impaired vascular function in vivo. Mice injected with DIO iPSC-ECs achieved significantly less reperfusion beginning at Day 10 compared with mice injected with control iPSC-ECs. While inflammation is often observed following surgical induction of hindlimb ischaemia (Silvestre et al. 2008), we observed significantly more inflammatory cells as well as muscle atrophy in mice injected with DIO iPSC-ECs compared with those injected with control iPSC-ECs. Immunostaining for $CD31^{+}$ cells also revealed significantly lower capillary density counts in the hindlimbs of mice injected with DIO iPSC-ECs compared with control iPSC-ECs. Microarray gene expression analysis comparing iPSC-ECs from control and DIO mice revealed 472 differentially regulated genes involved in biological pathways, including apoptosis, inflammation, immune function, oxidative stress, and cell senescence. Previous studies have demonstrated that statin treatment can promote angiogenesis in murine models of hindlimb ischaemia (Kureishi et al. 2000, Sata et al. 2001). In addition to their lipid lowering effects, statins can decrease inflammation and increase eNOS expression, resulting in a subsequent increase in NO bioavailability (Ni et al. 2001, Davignon 2004, Mason et al. 2004, Schonbeck and Libby 2004). In keeping with these observations, another important finding of this study is that co administration of low-dose pravastatin is able to reverse much of the dysfunc-

tion observed with DIO iPSC-ECs both in vitro and in vivo. Mechanistically, pravastatin therapy had significant beneficial effects in vitro on apoptosis, inflammation, and oxidative stress in DIO iPSC-ECs (Supplementary material, Figure S11). Pravastatin also resulted in a significant improvement in hindlimb reperfusion following ischaemia compared with mice receiving iPSC-ECs without pravastatin co-administration. These effects were inhibited by concurrent administration of L-NAME, an NO synthase inhibitor, suggesting the effects of pravastatin were via an NO-dependent mechanism. Taken together, these results correlate with a large body of evidence demonstrating that in pre-diabetes and DIO, abnormally high levels of inflammatory and oxidative stress biomarkers are associated with increased cellular apoptosis, leading to subsequent long-term complications such as endothelial dysfunction (van den Oever et al. 2010). These prolonged periods of heightened oxidative stress and inflammation can result in dysfunctional progenitor and stem cell populations, which have been implicated in increased risk of cardiovascular disease and PVD in patients with diabetes (Ohshima et al. 2009, Magenta et al. 2014). The observation that DIO iPSC-ECs show impaired function both in vitro and in vivo suggests one of the consequences of the altered metabolic state is the induction of global epigenetic changes that contribute to impaired EC function seen in these animals. These results are relevant and significant for cell therapy approaches. While autologous iPSC-ECs derived from obese patients might obviate issues associated with immunological rejection, these iPSC-ECs may be inadequate for restoring normal vascular function compared with iPSC-ECs derived from healthy donors. Based on these results, low-dose statin therapy may be a useful adjuvant when co-administered with dysfunctional DIO iPSC-ECs. Finally, the current iPSC-EC platform can also be used to identify additional novel drug targets that can alter the diabetes-induced dysfunctional state (Matsa et al. 2014).

In summary, our study is the first to show that iPSC-ECs derived from DIO mice exhibit decreased vascular function in vitro, and reduced function and incorporation into the host vasculature in vivo. Histological evaluation revealed muscle atrophy and increased infiltration of inflammatory cells in the ischaemic hindlimbs of mice receiving DIO iPSC-ECs. The EC dysfunction may be related to apoptosis, inflammation, and oxidative stress due to decreased NO production. Co administration with low-dose pravastatin therapy reversed EC dysfunction both in vitro and in vivo. Collectively, these findings may have important implications and caveats for future patient-specific iPSC-EC therapy, especially in pre-diabetic or DIO patients with PVD.

REFERENCES

Andrikopoulos, S., A. R. Blair, N. Deluca, B. C. Fam and J. Proietto (2008). "Evaluating the glucose tolerance test in mice." American journal of physiology. Endocrinology and metabolism 295(6): E1323-1332.

Birse, R. T., J. Choi, K. Reardon, J. Rodriguez, S. Graham, S. Diop, . . . S. Oldham (2010). "High-fat-diet-induced obesity and heart dysfunction are regulated by the TOR pathway in Drosophila." Cell Metab 12(5): 533-544.

Bruning, J. C., J. Winnay, B. Cheatham and C. R. Kahn (1997). "Differential signaling by insulin receptor substrate 1 (IRS-1) and IRS-2 in IRS-1-deficient cells." Molecular and cellular biology 17(3): 1513-1521.

Bruyndonckx, L., V. Hoymans, A. Van Craenenbroeck, D. Vissers, C. Vrints, J. Ramet and V. Conraads (2013). Assessment of Endothelial Dysfunction in Childhood Obesity and Clinical Use. Prevalence, Pathophysiology, and Management, Informa UK Limited: 165-206.

Burridge, P. W., D. Anderson, H. Priddle, M. D. Barbadillo Munoz, S. Chamberlain, C. Allegrucci, . . . C. Denning (2007). "Improved human embryonic stem cell embryoid body homogeneity and cardiomyocyte differentiation from a novel V-96 plate aggregation system highlights interline variability." Stem Cells 25(4): 929-938.

Caballero, A. E. (2003). "Endothelial dysfunction in obesity and insulin resistance: a road to diabetes and heart disease." Obes Res 11(11): 1278-1289.

Cho, S. W., S. H. Moon, S. H. Lee, S. W. Kang, J. Kim, J. M. Lim, . . . H. M. Chung (2007). "Improvement of postnatal neovascularization by human embryonic stem cell derived endothelial-like cell transplantation in a mouse model of hindlimb ischemia." Circulation 116(21): 2409-2419.

Davignon, J. (2004). "Beneficial cardiovascular pleiotropic effects of statins." Circulation 109(23 Suppl 1): III39-43.

Du, X., D. Edelstein, S. Obici, N. Higham, M. H. Zou and M. Brownlee (2006). "Insulin resistance reduces arterial prostacyclin synthase and eNOS activities by increasing endothelial fatty acid oxidation." J Clin Invest 116(4): 1071-1080.

Esposito, K., F. Nappo, R. Marfella, G. Giugliano, F. Giugliano, M. Ciotola, . . . D. Giugliano (2002). "Inflammatory cytokine concentrations are acutely increased by hyperglycemia in humans: role of oxidative stress." Circulation 106(16): 2067-2072.

Flegal, K. M., M. D. Carroll, C. L. Ogden and L. R. Curtin (2010). "Prevalence and trends in obesity among US adults, 1999-2008." JAMA 303(3): 235-241.

Galassetti, P. (2012). "Inflammation and oxidative stress in obesity, metabolic syndrome, and diabetes." Exp Diabetes Res 2012: 943706.

Guzik, T. J. (2002). "Mechanisms of Increased Vascular Superoxide Production in Human Diabetes Mellitus: Role of NAD(P)H Oxidase and Endothelial Nitric Oxide Synthase." Circulation 105(14): 1656-1662.

Hamelin, B. A. and J. Turgeon (1998). "Hydrophilicity/lipophilicity: relevance for the pharmacology and clinical effects of HMG-CoA reductase inhibitors." Trends Pharmacol Sci 19(1): 26-37.

Hink, U., H. Li, H. Mollnau, M. Oelze, E. Matheis, M. Hartmann, . . . T. Munzel (2001). "Mechanisms underlying endothelial dysfunction in diabetes mellitus." Circ Res 88(2): E14-22.

Huang, N. F., H. Niiyama, C. Peter, A. De, Y. Natkunam, F. Fleissner, . . . J. P. Cooke (2010). "Embryonic stem cell-derived endothelial cells engraft into the ischemic hindlimb and restore perfusion." Arterioscle-rosis, thrombosis, and vascular biology 30(5): 984-991.

Kobayashi, M., K. Inoue, E. Warabi, T. Minami and T. Kodama (2005). "A simple method of isolating mouse aortic endothelial cells." Journal of atherosclerosis and thrombosis 12(3): 138-142.

Kureishi, Y., Z. Luo, I. Shiojima, A. Bialik, D. Fulton, D. J. Lefer, . . . K. Walsh (2000). "The HMG-CoA reductase inhibitor simvastatin activates the protein kinase Akt and promotes angiogenesis in normocholesterolemic animals." Nat Med 6(9): 1004-1010.

Lai, W.-H., J. C. Y. Ho, Y.-C. Chan, J. H. L. Ng, K.-W. Au, L.-Y. Wong, . . . H.-F. Tse (2013). "Attenuation of Hind-Limb Ischemia in Mice with Endothelial-Like Cells Derived from Different Sources of Human Stem Cells." PLoS ONE 8(3): e57876.

Leber, A., B. Hemmens, B. Klosch, W. Goessler, G. Raber, B. Mayer and K. Schmidt (1999). "Characterization of recombinant human endothelial nitric-oxide synthase purified from the yeast Pichia pastoris." J Biol Chem 274(53): 37658-37664.

Li, Z., J. C. Wu, A. Y. Sheikh, D. Kraft, F. Cao, X. Xie, . . . J. P. Cooke (2007). "Differentiation, survival, and function of embryonic stem cell derived endothelial cells for ischemic heart disease." Circulation 116(11 Suppl): I46-54.

Liang, C. C., A. Y. Park and J. L. Guan (2007). "In vitro scratch assay: a convenient and inexpensive method for analysis of cell migration in vitro." Nature protocols 2(2): 329-333.

Limbourg, A., T. Korff, L. C. Napp, W. Schaper, H. Drexler and F. P. Limbourg (2009). "Evaluation of postnatal arteriogenesis and angiogenesis in a mouse model of hind-limb ischemia." Nature protocols 4(12): 1737-1746.

Liu, Y., J. Wei, S. Hu and L. Hu (2012). "Beneficial effects of statins on endothelial progenitor cells." Am J Med Sci 344(3): 220-226.

Maehr, R., S. Chen, M. Snitow, T. Ludwig, L. Yagasaki, R. Goland, . . . D. A. Melton (2009). "Generation of pluripotent stem cells from patients with type 1 diabetes." Proc Natl Acad Sci U S A 106(37): 15768-15773.

Magenta, A., S. Greco, M. C. Capogrossi, C. Gaetano and F. Martelli (2014). "Nitric Oxide, Oxidative Stress, andp66ShcInterplay in Diabetic Endothelial Dysfunction." BioMed Research International 2014: 1-16.

Mason, R. P., M. F. Walter and R. F. Jacob (2004). "Effects of HMG-CoA reductase inhibitors on endothelial function: role of microdomains and oxidative stress." Circulation 109(21 Suppl 1): II34-41.

Matsa, E., P. W. Burridge and J. C. Wu (2014). "Human Stem Cells for Modeling Heart Disease and for Drug Discovery." Science Translational Medicine 6(239): 239ps236-239ps236.

Michell, B. J. (2001). "Coordinated Control of Endothelial Nitric-oxide Synthase Phosphorylation by Protein Kinase C and the cAMP-dependent Protein Kinase." Journal of Biological Chemistry 276(21): 17625-17628.

Ni, W., K. Egashira, C. Kataoka, S. Kitamoto, M. Koyanagi, S. Inoue and A. Takeshita (2001). "Antiinflammatory and antiarteriosclerotic actions of HMG-CoA reductase inhibitors in a rat model of chronic inhibition of nitric oxide synthesis." Circ Res 89(5): 415-421.

Ohshima, M., T.-S. Li, M. Kubo, S.-L. Qin and K. Hamano (2009). "Antioxidant Therapy Attenuates Diabetes-Related Impairment of Bone Marrow Stem Cells." Circulation Journal 73(1): 162-166.

Reinhart-King, C. A. (2008). "Endothelial cell adhesion and migration." Methods in enzymology 443: 45-64.

Rodríguez-Crespo, I., P. Moënne-Loccoz, T. M. Loehr and P. R. Ortiz de Montellano (1997). "Endothelial Nitric Oxide Synthase: Modulations of the Distal Heme Site Produced by Progressive N-Terminal Deletions †." Biochemistry 36(28): 8530-8538.

Sansbury, B. E., T. D. Cummins, Y. Tang, J. Hellmann, C. R. Holden, M. A. Harbeson, . . . B. G. Hill (2012). "Overexpression of Endothelial Nitric Oxide Synthase Prevents Diet-Induced Obesity and Regulates Adipocyte Phenotype." Circulation Research 111(9): 1176-1189.

Sata, M., H. Nishimatsu, E. Suzuki, S. Sugiura, M. Yoshizumi, Y. Ouchi, . . . R. Nagai (2001). "Endothelial nitric oxide synthase is essential for the HMG-CoA reductase inhibitor cerivastatin to promote collateral growth in response to ischemia." FASEB J 15(13): 2530-2532.

Schonbeck, U. and P. Libby (2004). "Inflammation, immunity, and HMG-CoA reductase inhibitors: statins as antiinflammatory agents?" Circulation 109(21 Suppl 1): II18-26.

Silvestre, J. S., Z. Mallat, A. Tedgui and B. I. Levy (2008). "Post-ischaemic neovascularization and inflammation." Cardiovascular Research 78(2): 242-249.

Szendroedi, J. and M. Roden (2009). "Ectopic lipids and organ function." Curr Opin Lipidol 20(1): 50-56.

Takahashi, K., K. Tanabe, M. Ohnuki, M. Narita, T. Ichisaka, K. Tomoda and S. Yamanaka (2007). "Induction of pluripotent stem cells from adult human fibroblasts by defined factors." Cell 131(5): 861-872.

van den Oever, I. A., H. G. Raterman, M. T. Nurmohamed and S. Simsek (2010). "Endothelial dysfunction, inflammation, and apoptosis in diabetes mellitus." Mediators Inflamm 2010: 792393.

Voyta, J. C., D. P. Via, C. E. Butterfield and B. R. Zetter (1984). "Identification and isolation of endothelial cells based on their increased uptake of acetylated-low density lipoprotein." J Cell Biol 99(6): 2034-2040.

Wang, C. Y. and J. K. Liao (2012). "A mouse model of diet-induced obesity and insulin resistance." Methods in molecular biology 821: 421-433.

Warlich, E., J. Kuehle, T. Cantz, M. H. Brugman, T. Maetzig, M. Galla, . . . A. Schambach (2011). "Lentiviral vector design and imaging approaches to visualize the early stages of cellular reprogramming." Molecular therapy : the journal of the American Society of Gene Therapy 19(4): 782-789.

Weir, C., M. C. Morel-Kopp, A. Gill, K. Tinworth, L. Ladd, S. N. Hunyor and C. Ward (2008). "Mesenchymal stem cells: isolation, characterisation and in vivo fluorescent dye tracking." Heart, lung & circulation 17(5): 395-403.

Yamahara, K., M. Sone, H. Itoh, J. K. Yamashita, T. Yurugi-Kobayashi, K. Homma, . . . K. Nakao (2008). "Augmentation of Neovascularizaiton in Hindlimb Ischemia by Combined Transplantation of Human Embryonic Stem Cells-Derived Endothelial and Mural Cells." PLoS ONE 3(2): e1666.

Yamashita, J., H. Itoh, M. Hirashima, M. Ogawa, S. Nishikawa, T. Yurugi, . . . S. Nishikawa (2000). "Flk1-positive cells derived from embryonic stem cells serve as vascular progenitors." Nature 408(6808): 92-96.

Yu, J., N. F. Huang, K. D. Wilson, J. B. Velotta, M. Huang, Z. Li, . . . J. C. Wu (2009). "nAChRs mediate human embryonic stem cell-derived endothelial cells: proliferation, apoptosis, and angiogenesis." PLoS One 4(9): e7040.

Zou, M.-H., C. Shi and R. A. Cohen (2002). "Oxidation of the zinc-thiolate complex and uncoupling of endothelial nitric oxide synthase by peroxynitrite." Journal of Clinical Investigation 109(6): 817-826.

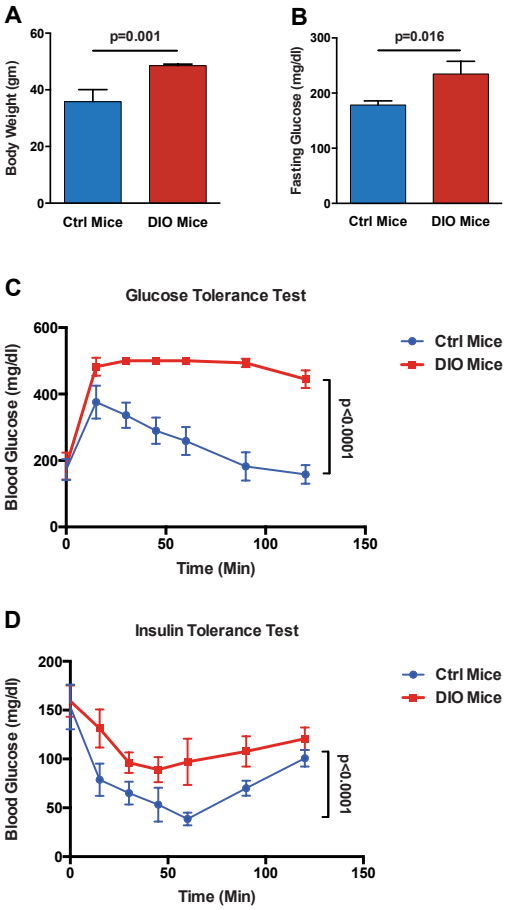

Supplementary Figure 1. Comparisons of control and DIO mice. (A) DIO mice had a significantly higher body weight (p=0.001) and (B) fasting blood glucose (p=0.016) compared to control mice. (C) DIO mice exhibited a significant decrease in glucose tolerance (p<0.001) and (D) insulin tolerance compared to control mice (p<0.001).

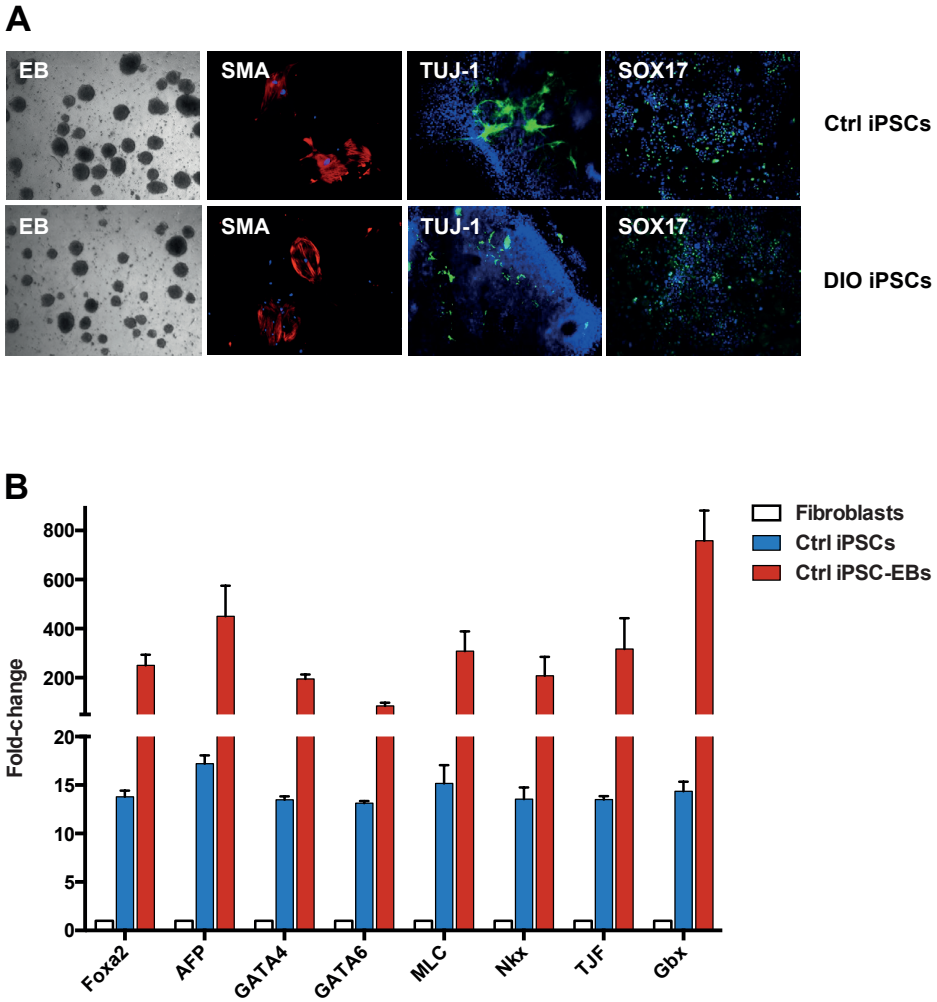

Supplementary Figure 2. Characterization of murine iPSCs. (A) Following embryoid body (EB) formation, outgrowths generated from iPSCs derived from control and DIO mice expressed markers of the three germ layers: mesoderm (SMA), ectoderm (TUJ-1), and endoderm (SOX17). (B) RT-PCR performed on RNAs isolated from differentiated EBs of control iPSCs confirmed expression of genes specific for the three germ layers (mesoderm, ectoderm, and endoderm). Fold-change compared to fibroblasts.

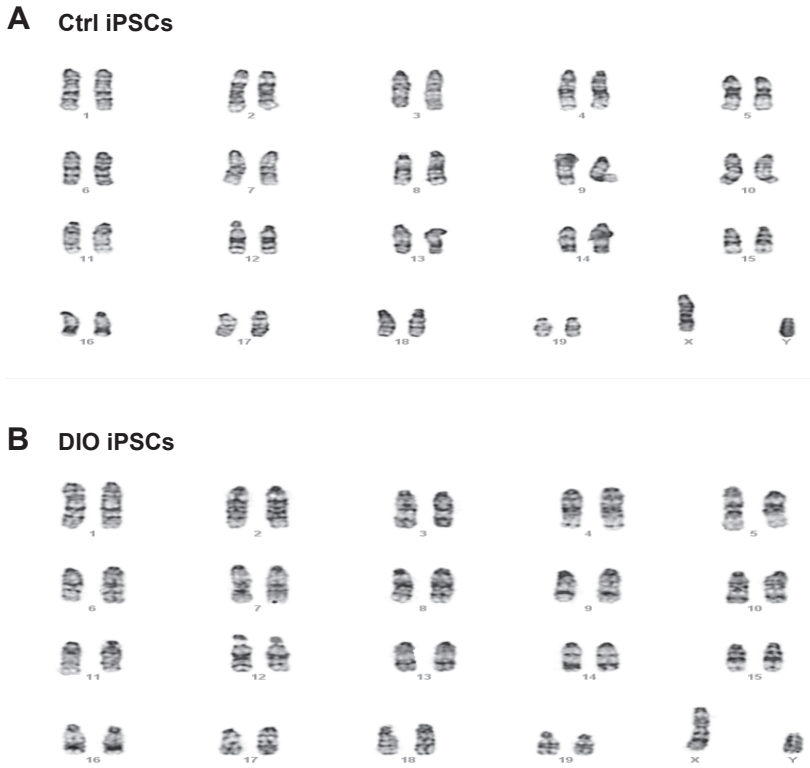

Supplementary Figure 3. Karyotype analysis of murine iPSCs. (A) iPSC lines derived from control and (B) DIO mice maintained a normal karyotype after extended passage.

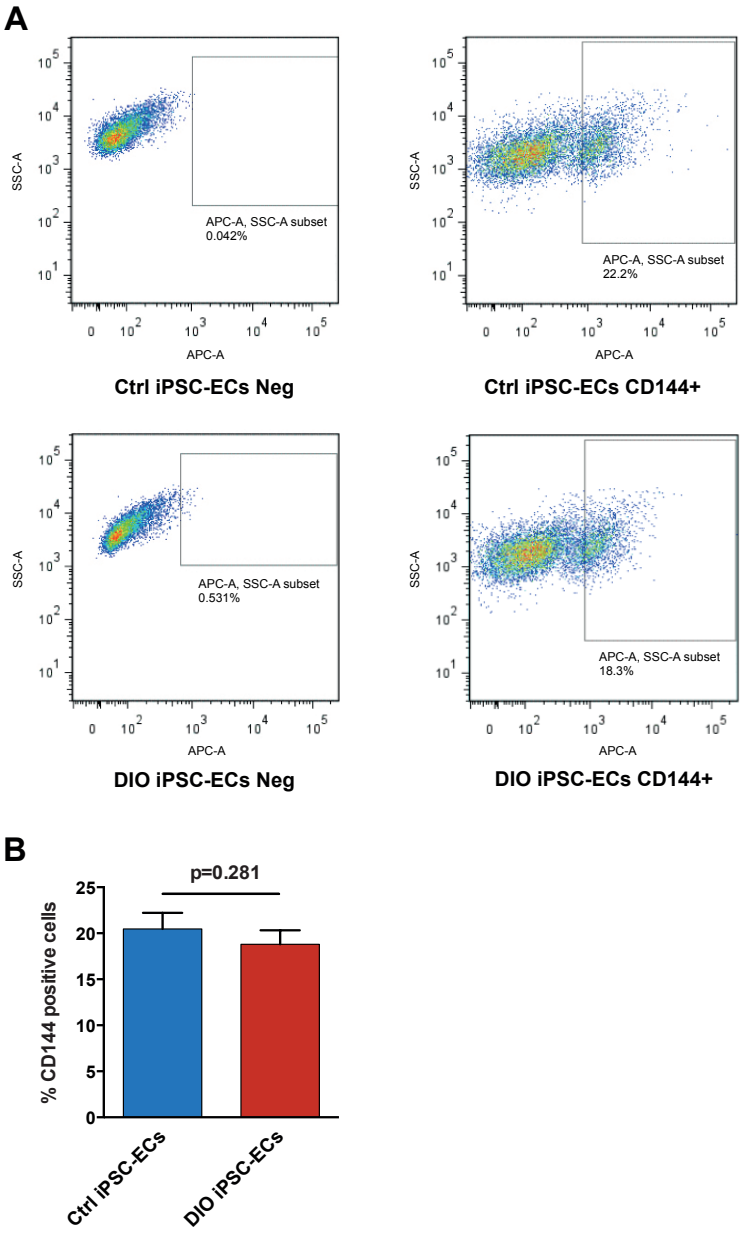

Supplementary Figure 4. Flow cytometry analysis of iPSC-EC differentiation efficiency. (A) Dot plots of iPSC-ECs stained with anti CD144-APC conjugated antibody in both control mice (upper panel) and DIO mice (lower panel). (B) Quantification of flow cytometry showed no significant differences in iPSC-EC differentiation efficiency between control and DIO group (20.47%±1.75% vs. 18.80%±1.51%, Ctrl iPSC-ECs vs. DIO iPSC-ECs, p=0.281).

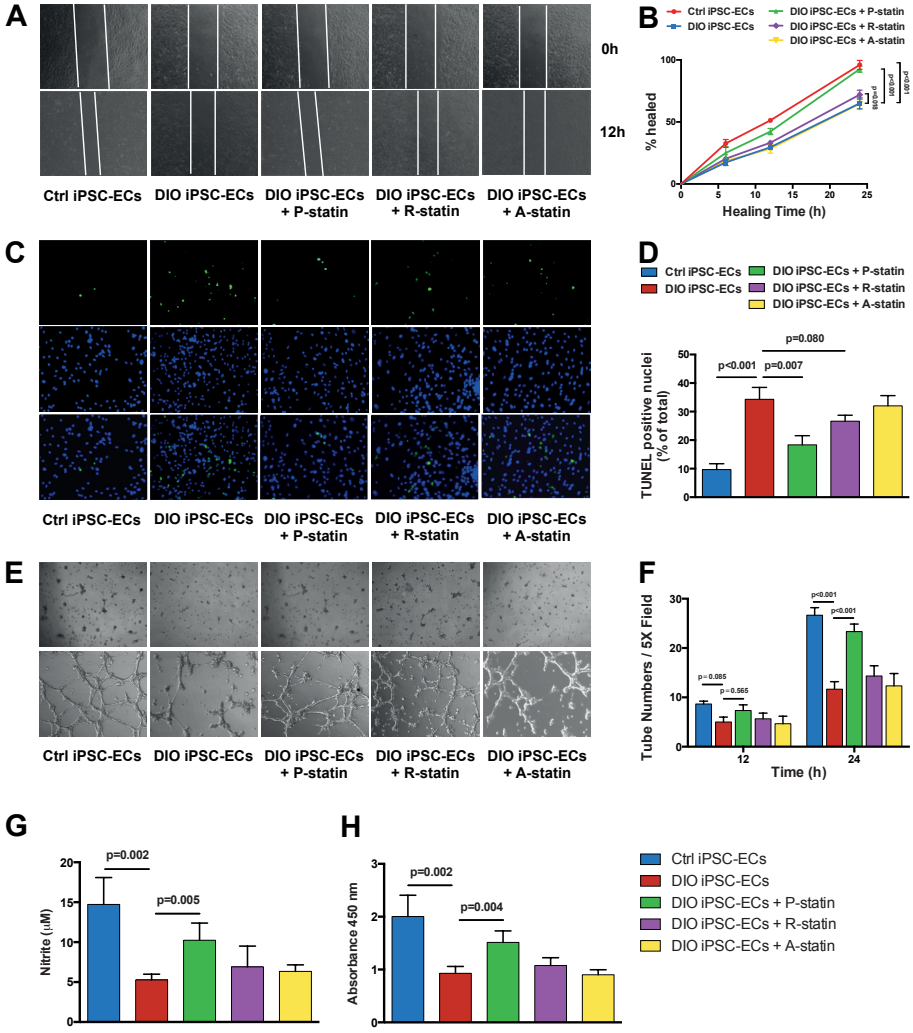

Supplementary Figure 5. Comparison of endothelial function recovery after pravastatin, rosuvastatin, and atorvastatin treatment in DIO iPSC-ECs. (A-B) iPSC-ECs from DIO mice demonstrated significant reductions in cell migration ($p<0.001$). Treatment with pravastatin (P- Statin) and rosuvastatin (R-Statin) reversed this phenotype ($p<0.001$ DIO iPSC-ECs vs. DIO iPSC-ECs + P-statin; $p=0.018$ DIO iPSC-ECs vs. DIO iPSC-ECs + R-statin). (C-D) TUNEL staining showed that P-statin and R-statin protected DIO iPSC-ECs from hypoxia-induced apoptosis ($p=0.007$ DIO iPSC-ECs vs. DIO iPSC-ECs + P-statin; $p=0.08$ DIO iPSC-ECs vs. DIO iPSC-ECs + R-statin). (E-F) P-statin treatment increased capacity to form a capillary-like network on Matrigel after 24 hours compared to DIO iPSC-ECs ($p<0.001$). However, the addition of R-statin and A-statin failed to significantly increase the capillary-like network in DIO iPSC-ECs. (G) Measurement of nitrite levels in cell culture supernatant by Griess reaction demonstrated that DIO iPSC-ECs had significantly lower levels of nitric oxide production compared to control iPSC-ECs ($p=0.002$), where incubation of DIO iPSC-ECs with P-statin for 24 hours resulted in significantly higher levels of NO ($p=0.005$). Incubation with R-statin and A- statin did not significantly change the NO production in DIO iPSC-ECs. (H) P-statin treatment significantly increased the cell proliferation rate in DIO iPSC-ECs ($p=0.004$), while R-statin and A-statin showed no significant protective effect.

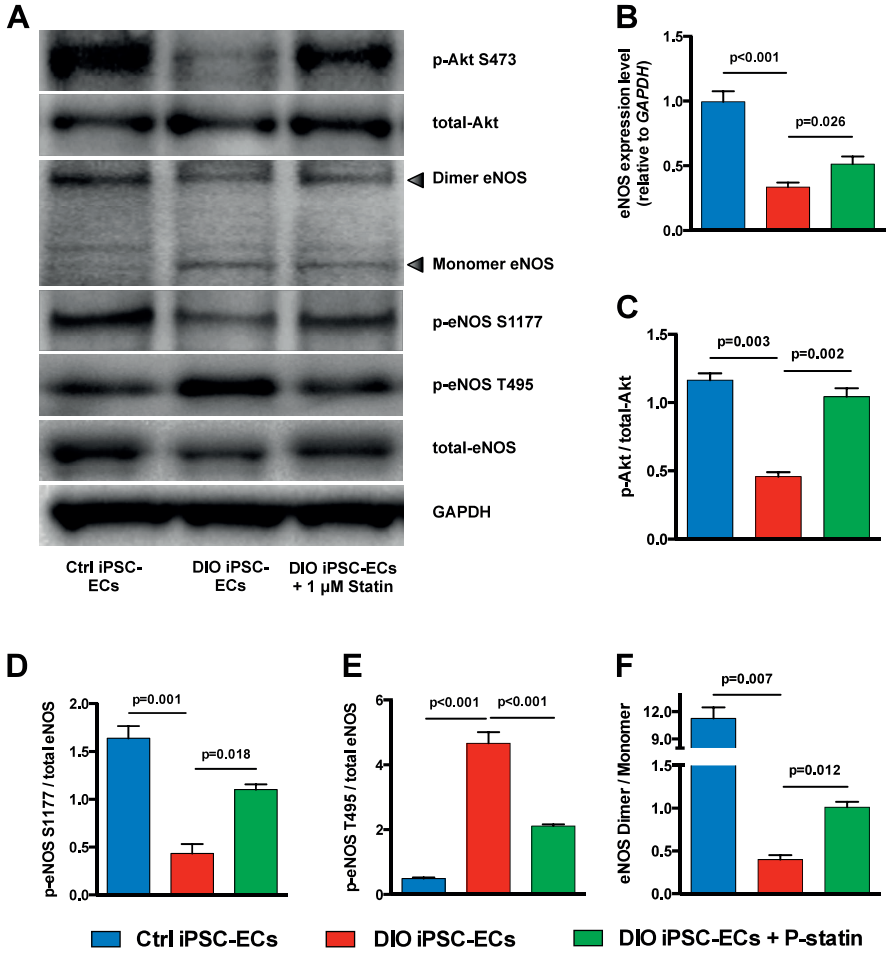

Supplementary Figure 6. eNOS protein levels, phosphorylation status, and dimerization in control iPSC-ECs and DIO iPSC-ECs. (A) Representative western blots and quantification of protein from control iPSC-ECs, DIO iPSC-ECs, and DIO iPSC-ECs with pravastatin treatment for 24 hours probed with (B) antibodies recognizing total eNOS protein, (C) antibodies recognizing serine phosphorylation of residue 473 of Akt protein and total Akt protein, (D) serine phosphorylation of residue 1177 of eNOS, or (E) threonine phosphorylation of residue 495 of eNOS. (F) eNOS dimers and monomers were separated by low-temperature SDS-PAGE (3- 8%) and the membrane was probed with eNOS antibody. The intensity (area times density) of dimers and monomers was determined by densitometry as described in Supplementary Methods. The results were expressed as eNOS dimer to monomer ratio. All blots were stripped and re- probed with an antibody to GAPDH (bottom) and blot shown is representative of three independent experiments.

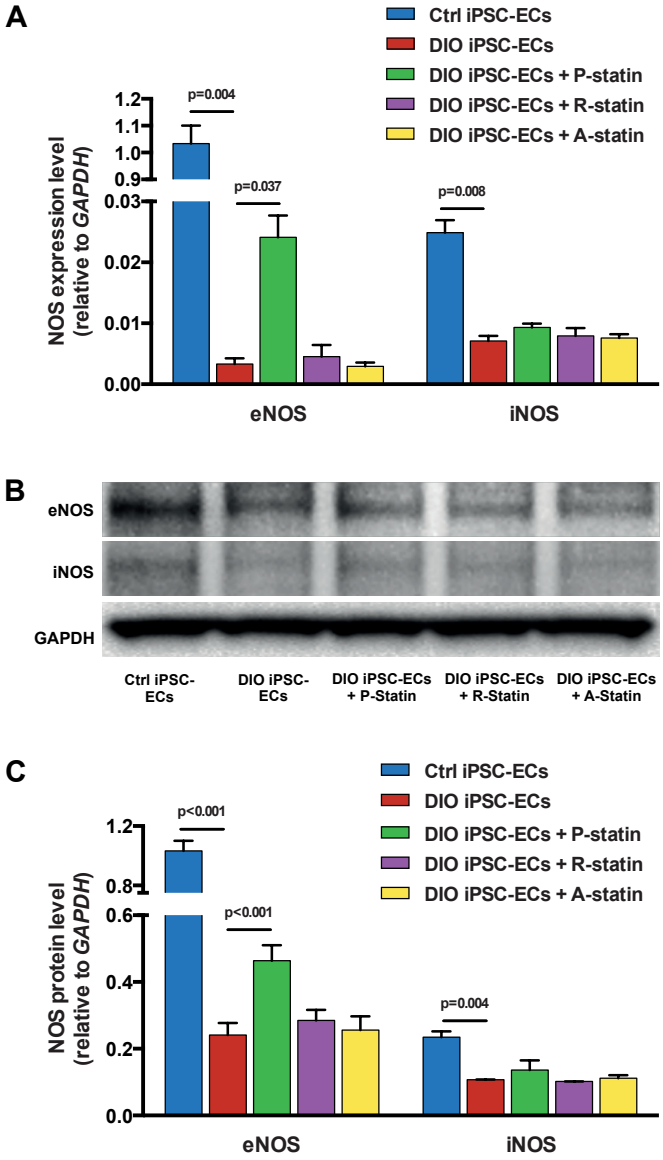

Supplementary Figure 7. eNOS and iNOS gene expression in control and DIO iPSC-ECs. (A) Real-time PCR was performed on cDNAs from control iPSC-ECs, DIO iPSC-ECs, and DIO iPSC-ECs following statin treatments. At basal level, control iPSC-ECs expressed more eNOS (p=0.004) and iNOS (p=0.008) compared with DIO iPSC-ECs. Incubation with pravastatin for 24 hours significantly increased eNOS gene expression in DIO iPSC-ECs (p=0.037 DIO iPSC- ECs vs. DIO iPSC-ECs + P-statin). None of the three statins showed any significant effect on iNOS gene expression in DIO iPSC-ECs at the transcriptional level. (B) Representative western blot images and (C) quantification of protein bands showed consistent results as gene expression assay. Both eNOS (p<0.001) and iNOS (p=0.004) protein levels were significantly reduced in DIO iPSC-ECs compared with control iPSC-ECs, while P-statin treatment only increased eNOS protein level in DIO iPSC-ECs (p<0.001, DIO iPSC-ECs vs. DIO iPSC-ECs + P-statin).

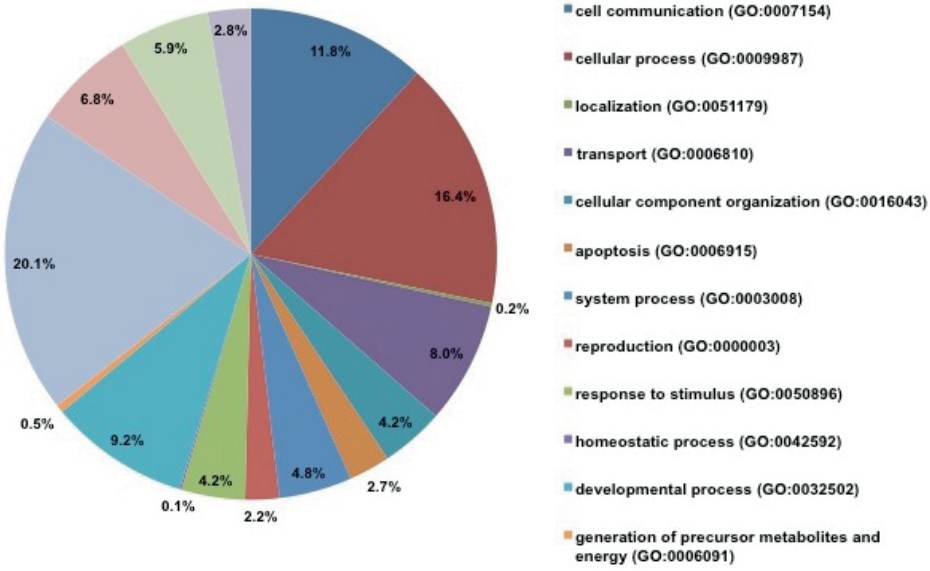

Supplementary Figure 8. Gene ontology (GO) biological pathway analysis. When comparing iPSC-ECs from control and DIO mice, GO biological pathway analysis identified the involvement of biological pathways including metabolism, cell cycle, immune function, inflammation, cell adhesion, oxidative stress, and apoptosis.

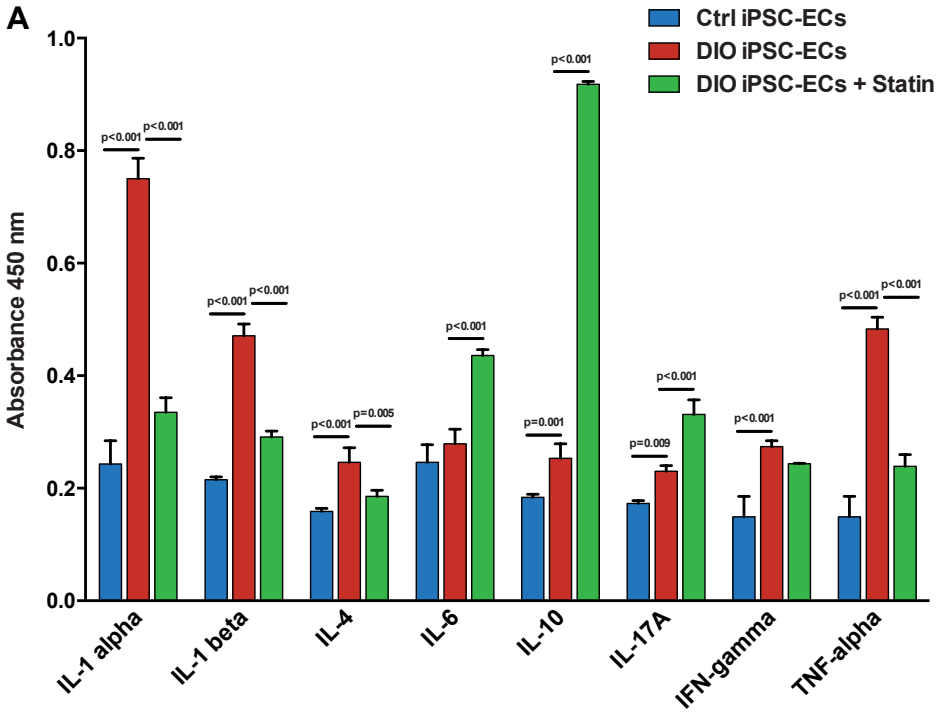

Supplementary Figure 9. Cell culture supernatants from DIO iPSC-ECs in hypoxia for 24 hours had significantly higher levels of the pro-inflammatory cytokines IL-1α, IL-1β, IL-4, IFN-γ, and TNF-α compared to control iPSC-ECs. Treatment of DIO iPSC-ECs with 1 uM pravastatin for 24 hours resulted in significant decreases in the pro-inflammatory cytokines IL-1α, IL-1β, IL-4, and TNF-α, and significant increases in anti-inflammatory cytokines IL-6, IL-10, and IL-17A (n=5/group).

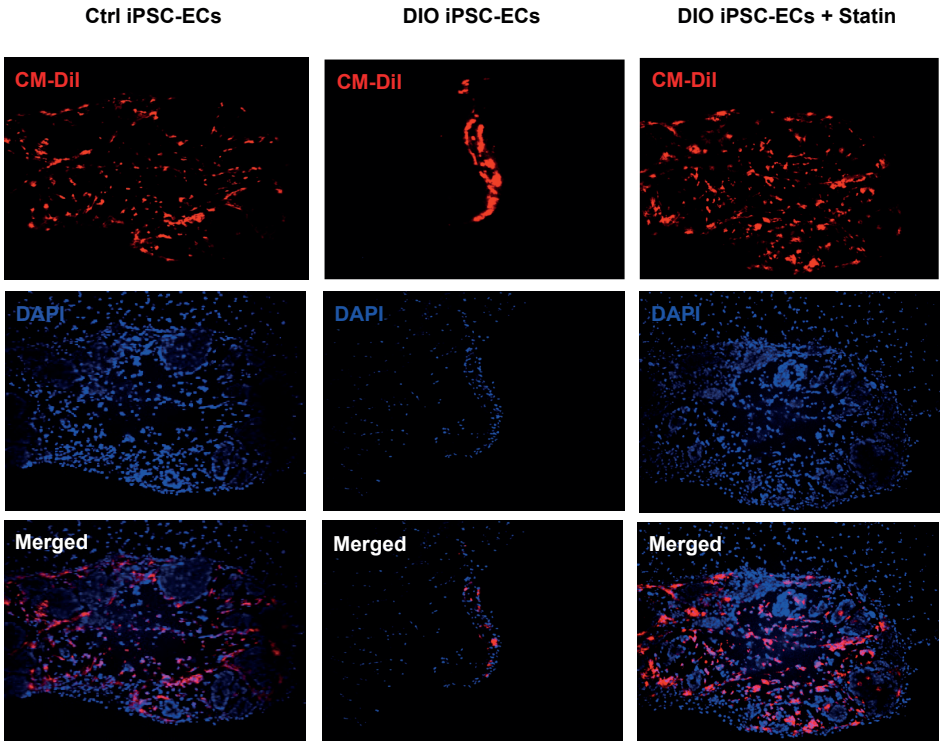

Supplementary Figure 10. Immunofluorescent staining for CM-DiI labeled iPSC-ECs. At day 14, there was significantly less fluorescent signal detected in all of the ischemic hindlimbs of mice injected with DIO iPSC-ECs compared to those injected with control iPSC-ECs.

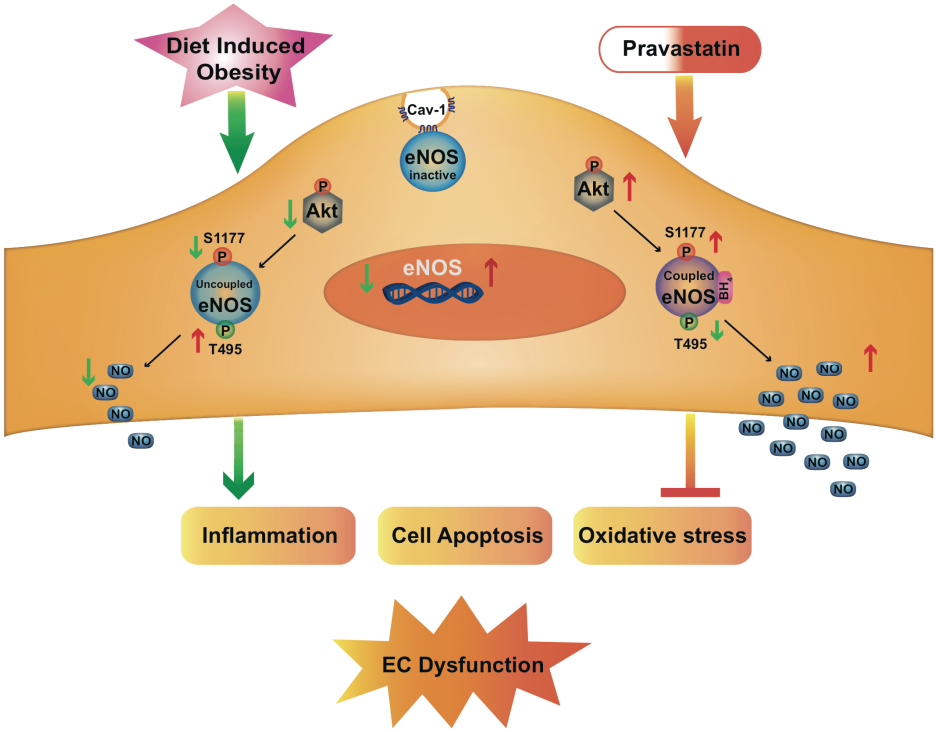

Supplementary Figure 11. Schematic representation of endothelial dysfunction associated with diet-induced obesity. Compared with iPSC-ECs from control mice, iPSC-ECs derived from obese mice showed 1) decreased Akt phosphorylation, which led to the reduction of eNOS phosphorylation at ser1177 residue; 2) increased eNOS phosphorylation at thr495 residue; 3) decreased eNOS gene expression and protein level; and 4) increased eNOS uncoupling. All of the above led to the deactivation of eNOS and reduced NO production in DIO iPSC-ECs, causing increased endothelial inflammation, cell apoptosis, and oxidative stress, thus resulting in EC dysfunction. Co-administration of 1 μM pravastatin therapy with DIO iPSC-ECs reversed this EC dysfunction through activation of eNOS signaling pathway.

Primers	Sequences (5'-3')
Foxa2	F: TAAGCGAGCTAAAGGGAGCA R: GTGGTTGAAGGCGTAATGGT
AFP	F: CGCGTTTCTGGTTGCTTACAC R: ACTTCTTGCTCTTGGCCTTGG
GATA4	F: TCTCACTATGGGCACAGCAG R: GCGATGTCTGAGTGACAGGA
GATA6	F: CATTTGGAGGAAACCGTGAA R: CCAGCAAATGCAGATTCCTT
MLC	F: CCACTCTGGGTGAGAGGCTA R: GGGCTGCCGTAGGATTCTC
Nkx	F: CCAAGGACCCTCGAGCTGA R: CGACAGATACCGCTGCTGCT
TJF	F: CGAGACCTACTGCATCGACA R: CATTGAGCTGACCAGGGAAT
Gbx	F: TGCAGGCGTCGCTCGTAG R: TCCGAGCTGTAGTCCAGATCA
18s	F: AAACGGCTACCACATCCAAG R: CCTCCAATGGATCCTCGTTA

Supplementary Table 1. Primer sequences for evaluating pluripotency by RT-PCR. A list of primer sequences used to confirm murine iPSCs can successfully differentiate into the three embryonic germ layers.

A

Gene	DIO iPSC-ECs / Ctrl iPSC-ECs	DIO iPSC-ECs + Statin / DIO iPSC-ECs	DIO iPSC-ECs + Statin / Ctrl iPSC-ECs
Bcl2a1a	5.57	-13.59	-2.44
Bcl2l10	14.06	-22.81	-1.62
Birc5	3.11	-4.73	-1.52
Bnip3	4.65	-17.59	-3.78
Bnip3l	4.68	-3.86	1.21
Casp3	3.52	-4.17	-1.18
Casp4	3.17	-3.35	-1.06
Cd40	4.30	-187.12	-43.53
Cd40lg	32.92	-43.92	-1.33
Cd70	4.62	-17.16	-3.72
Cidea	4.39	-72.11	-16.42
Dffb	4.08	-37.07	-9.08
Fas	6.98	-1.41	4.96
Fasl	4.68	-13.74	-2.93
Lhx4	5.98	-21.62	-3.62
Naip1	9.58	-12.42	-1.30
Nme5	3.12	-1.67	1.86
Polb	3.02	-4.51	-1.49
Prdx2	4.67	-7.88	-1.69
Pycard	4.64	2.03	9.41
Tnfsf10	6.60	-4.37	1.51
Traf1	4.90	-2.00	2.46

B

Gene	DIO iPSC-ECs / Ctrl iPSC-ECs	DIO iPSC-ECs + Statin / DIO iPSC-ECs	DIO iPSC-ECs + Statin / Ctrl iPSC-ECs
Als2	7.46	2.12	7.88
Atr	4.63	-161.92	-34.91
Duox1	6.80	-23.19	-3.40
Ehd2	3.27	1.69	6.56
Ercc2	3.99	2.01	8.02
Ercc6	3.40	-1.07	1.70
Gpx6	3.15	-473.39	-150.70
Gpx7	10.14	-9.50	1.07
Nqo1	3.00	-1.10	1.98
Vim	3.92	-1.97	1.15
Xpa	5.77	2.58	7.41

Supplementary Table 2. RT-PCR analysis of control, DIO iPSC-ECs, and DIO iPSC-ECs treated with 1 μM pravastatin for 24 hours. Of the genes investigated in panels consisting of (A) apoptotic and (B) oxidative stress pathway genes, 33 genes were significantly up-regulated (>3- fold) in DIO iPSC-ECs compared to control iPSC-ECs. After pravastatin treatment, 28 apoptotic and oxidative genes were down-regulated in DIO iPSC-ECs compared with untreated cells.